POWER REACTOR TECHNOLOGY

A Quarterly Technical Progress Review

Prepared by DIVISION OF TECHNICAL INFORMATION, USAEC,
in cooperation with COMBUSTION ENGINEERING, INC., NUCLEAR DIVISION

Summer 1965

● VOLUME 8

● NUMBER 3

TECHNICAL PROGRESS REVIEWS

To meet the needs of industry for concise summaries of current atomic developments, the Atomic Energy Commission is publishing this series, Technical Progress Reviews. Issued quarterly, each of the reviews digests and evaluates the latest findings in a specific area of nuclear technology and science.

The five journals published in this series are:

Isotopes and Radiation Technology, P. S. Baker, A. F. Rupp, and associates, Oak Ridge National Laboratory

Nuclear Safety, Wm. B. Cottrell, W. H. Jordan, and associates, Oak Ridge National Laboratory

Power Reactor Technology, formerly prepared and edited by W. H. Zinn and J. R. Dietrich, Nuclear Division, Combustion Engineering, Inc. (a new contractor will take over preparation of this journal beginning with Vol. 8, No. 4).

Reactor Fuel Processing, Stephen Lawroski and associates, Chemical Engineering Division, Argonne National Laboratory

Reactor Materials, R. W. Dayton, E. M. Simons, and associates, Battelle Memorial Institute

Each journal may be purchased from the Superintendent of Documents, U. S. Government Printing Office, Washington, D. C., 20402. *Isotopes and Radiation Technology* at $2.00 per year for subscription or $0.55 for individual issues; the other four journals at $2.50 per year and $0.70 per issue. See back cover for remittance instructions and foreign postage requirements.

Availability of Reports Cited in This Review

Unclassified AEC reports are available for inspection at AEC depository libraries and are sold by the Clearinghouse for Federal Scientific and Technical Information, National Bureau of Standards, U. S. Department of Commerce, 5285 Port Royal Road, Springfield, Va., 22151. Some of the reports cited are not available owing to their preliminary nature; however, the information contained in them will eventually be made available in formal progress or topical reports.

Unclassified reports issued by other Government agencies or private organizations should be requested from the originator.

Unclassified British and Canadian reports may be inspected at AEC depository libraries. British reports are sold by the British Information Service, 45 Rockefeller Plaza, New York, N. Y.; Canadian reports (AECL series) are sold by the Scientific Document Distribution Office, Atomic Energy of Canada, Ltd., Chalk River, Ontario, Canada.

Classified U. S. and foreign reports identified in this journal as Classified may be purchased by properly cleared Access Permit Holders from the Division of Technical Information Extension, U. S. Atomic Energy Commission, P. O. Box 1001, Oak Ridge, Tenn., 37831. Such reports may be inspected at classified AEC depository libraries.

POWER REACTOR TECHNOLOGY

A REVIEW OF RECENT DEVELOPMENTS

Prepared by DIVISION OF TECHNICAL INFORMATION, USAEC,
in cooperation with
COMBUSTION ENGINEERING, INC., NUCLEAR DIVISION

SUMMER 1965

VOLUME 8

NUMBER 3

Foreword

This is an interim quarterly review assembled by the Division of Technical Information, U. S. Atomic Energy Commission, from material supplied by Combustion Engineering, Inc., prior to the termination, at their request, of their contract to prepare the review. A new contractor will assume responsibility for the preparation of *Power Reactor Technology* beginning with the Fall issue, Vol. 8, No. 4.

Power Reactor Technology contains reviews of selected recently published reports that are judged noteworthy in the fields of power-reactor research and development, power-reactor applications, design practice, and operating experience. It is not meant to be a comprehensive abstract of all material published during the quarter, nor is it meant to be a treatise on any part of the subject. However, related reports from different sources are often treated together to yield reviews having some breadth of scope, and background material may be added to place recent developments in perspective. Occasionally the reviews are written by guest authors. Reviews having unusual breadth or significance are placed at the front of the issue as Feature Articles.

The intention is to cover the various areas of reactor development from the general viewpoint of the reactor designer rather than from the more detailed points of view of specialists in the individual areas. To whatever extent the coverage of *Power Reactor Technology* may occasionally overlap the fields of the other Technical Progress Reviews, the overlaps will be motivated by this objective of viewing current progress through the eyes of the reactor designer.

A degree of critical appraisal and some interpretation of results are often necessary to define the significance of reported work. Any such appraisal or interpretation represents only the opinion of the reviewer. Readers are urged to consult the original references to obtain all the background of the work reported and to obtain the interpretation of the results given by the original authors.

For timely coverage, *Power Reactor Technology* must often review fragmentary material. The fixed subject headings listed below have been adopted in the hope of maintaining some continuity and order in the material from one issue to another; all reviews except Feature Articles will be arranged under these headings. A particular issue will not necessarily contain all the headings but only those under which material is reviewed.

Economics, Applications, Programs
Resources and Fuel Cycles
Physics
Fluid and Thermal Technology
Fuel Elements
Materials
Control and Dynamics
Containment, Radiation Control, and Siting
Systems Technology
Components
Design and Construction Practice
Operating Experience
Specific Reactor Types
Specific Applications
Unconventional Approaches

U. S. Atomic Energy Commission
Division of Technical Information

Contents

NOTE: The Commission regrets to announce that, at the request of Combustion Engineering, Inc., their contract to prepare *Power Reactor Technology* has been terminated. This issue was assembled by the AEC Division of Technical Information from material supplied by Combustion prior to the time the contract expired. A new contractor, Argonne National Laboratory, will assume responsibility for preparation of *Power Reactor Technology* beginning with Vol. 8, No. 4, and the distribution of that issue will be delayed. Please direct any communications regarding this issue to the USAEC Division of Technical Information, Washington, D. C., 20545.

Issued quarterly by the U. S. Atomic Energy Commission. Use of funds for printing this publication approved by the Director of the Bureau of the Budget on October 14, 1963.

Section

I

Power Reactor Technology

Physics

Measurements on Operating Reactors

On installation of the second core in the Sodium Reactor Experiment (SRE), a test program was initiated to develop and evaluate techniques for measuring the nuclear parameters of the core and for checking core stability. An objective of this program is to make possible reliable interpretation of measured changes in control-rod positions in terms of reactivity values. A method of monitoring for abnormal behavior would then be available from the comparison of calculated and measured reactivity variations. References 1 and 2 describe some of the work directed toward this purpose.

Reference 1 presents test results that show the feasibility of a technique developed for calibrating shim rods during normal reactor power operation. When compared with other rod-calibration methods that have been used in the past, the new technique is said to have the following advantages: (1) increased plant availability, (2) elimination of operational hazards, (3) use of inexpensive equipment, and (4) elimination of special devices to drive the control rod or elimination of the need for a pile oscillator within the core. The technique utilizes an analog computer that is programmed to simulate the reactor. Six groups of delayed neutrons with a fuel-temperature feedback loop are included in the simulation. For a rod-calibration measurement, the reactor flux is manually cycled by moving the shim rod in equal increments about the critical position. A signal is taken from the shim-rod position indicator and is scaled with a potentiometer to give the shim-rod differential worth, which becomes the reactivity input for the computer. The computer output is the simulated-reactor-flux signal. The differences in actual reactor flux and simulated reactor flux are recorded on a strip chart. The shim-rod differential worth is given by the setting of the shim-rod-worth potentiometer, which results in agreement of the computer-flux response with the actual reactor-flux response. In practice the fuel-temperature feedback constants in the simulation circuit are adjusted until the system indicates the same differential rod worth for all frequencies of rod travel. Results of tests at 12 Mw(t) show that rod worths can be determined within ±5% of the true value. This compares with resolutions of ±2% obtained at zero power with normal period-measurement techniques. Reactor-flux noise was an important limiting factor to the attainment of higher accuracy with the on-line shim-rod-calibration technique.

Reference 2 describes the experiments performed to obtain the reactivity coefficients of core 2 of the SRE. From the results of transfer-function measurements at 10, 15, and 20 Mw(t), it was clearly demonstrated that the positive prompt power coefficient associated with fuel-rod bowing was eliminated when the clusters were constrained to prevent bowing. Through analyses of the reactivity variations introduced by a flow ramp and an inlet temperature ramp, the combined fuel-and-coolant temperature coefficient and the inlet temperature coefficient were determined. The combined coefficient was found to be −0.12 cents/°F, a value that agrees very well with the sum of the calculated Doppler and coolant coefficients. A simple lag model was used in the analysis of the inlet-temperature-ramp data. Although good agreement with calculations was obtained, it is recognized that the simple model used is not entirely adequate because the slow change in inlet temperature used in the experiment results in interactions with the reactivities associated with core temperatures. Other pertinent measurements are described, e.g., shim-rod

calibrations, xenon transient, and isothermal core temperature.

Reference 3 presents the results of a number of performance tests conducted at the Plutonium Recycle Test Reactor to investigate the operating characteristics of the plutonium-fueled D_2O-moderated reactor. The test results were obtained during initial operation with a three-zone configuration comprising natural UO_2 elements in the central region surrounded by an annulus of plutonium-aluminum elements and an outer region of UO_2 elements. Reactor refuelings to compensate for burnup were made by charging fresh plutonium-aluminum elements in the intermediate zone. When a steady-state loading was finally achieved, the intermediate plutonium-aluminum zone was somewhat expanded, as compared to the initial loading, at the expense of a reduced central zone of the UO_2 elements. Measurements were made of the change in reactivity with fuel burnup. The rate of loss of reactivity per unit of energy production increased with the inventory of plutonium in the reactor, as expected from the results of diffusion-theory perturbation calculations. As the steady-state loading was approached, the fraction of the total core fissions rate due to the plutonium was about 55%.

Measurements were made of the radial power distribution by computing individual tube power outputs from flow and temperature-rise data; data are presented for exposures of 0, 1000, and 2000 Mwd. As a result of the method of charging the plutonium-aluminum elements in the intermediate zone of the three-zone core (outside-in method), the radial power flattening improved with increasing exposure.

Measurements of the photoneutron flux were observed to decay at a rate determined by a fission-product decay curve derived from the work of Perkins and King;[4] the curve represented a simulation of the decay rate of gamma flux from the emitters giving gammas of energy greater than 2.2 Mev, the threshold energy for the (γ,n) reaction in deuterium. Measurements of the shim-rod worths, using the partial water-height method, showed decreasing total worth as operation of the reactor progressed to the steady-state three-zone fuel loading, i.e., as the plutonium-fission ratio increased. Random-noise techniques were used to measure the reactor transfer function and thus to obtain β/l. The measurements indicated a decrease in β/l as the plutonium inventory in the reactor was increased. The combined fuel-plus-coolant temperature coefficient and the moderator temperature coefficient were observed to become much less negative as the plutonium inventory was increased during the approach to the steady-state configuration. A contributing factor to the decreases in negative temperature coefficients was the gradual degradation of the primary coolant from 99.75% to 95% D_2O during the course of reactor operation. The decreases in negative coefficient values were not considered large enough to affect reactor safety.

References 5 and 6 report on the recent successful operation of the Experimental Breeder Reactor No. 1 (EBR-I) with a plutonium loading (Mark IV). The results of a stability analysis, based essentially on transfer-function and power-coefficient measurements, are presented in Ref. 5, wherein it is noted that there is nothing inherently unsafe or dangerous in the operation of a plutonium-fueled system. The results of breeding-gain measurements, which demonstrate directly the superiority of plutonium as a fuel, are treated in Ref. 6.

Oscillator-rod measurements were conducted on EBR-I, Mark IV, to obtain the zero-power and load-power transfer functions. From the transfer functions a separation was made of the reactivity feedback corresponding to the various reactor power levels and inlet coolant temperatures. Reference 5 describes the reactivity-feedback function by a mathematical model characterized by the following two terms: (1) prompt, small, and associated primarily with power changes in the fuel (axial expansion of fuel, NaK expulsion, radial expansion of the Zircaloy jackets, fuel-slug bowing, and jacket bowing); and (2) relatively delayed, strong, and associated with expansion effects in the coolant, structure, and upper portion of the blanket region. Substitution of the experimental data into the mathematical model results in a set of time constants and power coefficients that adequately describes the experimentally derived reactivity-feedback function for a given set of operating conditions. In all cases the values of the fitted time constants are consistent with values estimated from heat-transfer considerations.

The fitted power-coefficient values for the delayed term greatly exceed the corresponding values established for the prompt fuel-

expansion term. This empirical result is surprising and is attributed to slug-bowing effects that cancel nearly all the usual prompt negative effects. That slug bowing is an important mechanism is also indicated by the static measurements of the power coefficient. Insofar as the stability and safety of the system are concerned, it is concluded that the effects of slug bowing are not particularly important. In all cases studied the overall power coefficient was strongly negative and was still sufficiently rapid in action to prevent strong reinforcement of input and feedback reactivities. Changes in coolant inlet temperature were found to effect strong changes in the feedback, apparently a consequence of temperature-sensitive clearances.

Reference 5 concludes that, in general, a system fueled with plutonium would tend to be more sensitive to reactivity perturbations than one fueled with uranium. For a feedback that reinforces the input, the neutron kinetics are such that the system tends to be less stable (relative to ^{235}U fuel). However, for a feedback that cancels a portion of the input, the system would tend to be more stable. Hence, if slug-bowing and rod-bowing effects could be eliminated, it is possible that the kinetic behavior of a plutonium-fueled system would be more stable than that of its ^{235}U-fueled counterpart.

The experimental methods used for the breeding-gain measurements on EBR-I, Mark IV, are described in detail in Ref. 6. The method is based on integration of the various fission and capture patterns over the system volume. The mapping technique requires observation of activities generated in thin metallic foils of uranium and plutonium inserted in the core and blanket regions of the assembly. The counting operations for the various types of foils and the operations involved in the organization of the counting data for integration purposes are described. Spatial distributions were established for plutonium, ^{235}U, and ^{238}U fissions and captures. It should be noted that specific measurements of captures in plutonium and ^{235}U were not carried out on the Mark IV loading. Instead, use was made of the results of measurements by Kafalas et al.,[7] who established values of α for ^{239}Pu and ^{235}U as a function of radial distance and elevation in a ^{235}U-fueled loading in EBR-I.

The breeding ratio is defined as the ratio of ^{239}Pu and ^{241}Pu production to ^{235}U, ^{239}Pu, and ^{241}Pu destruction. The value of breeding ratio arrived at from the measurements is 1.27 ± 0.08. This value demonstrates the importance of ^{239}Pu as a fast reactor fuel since earlier measurements of the conversion ratio of essentially the same system fueled with ^{235}U gave values of the order of unity. The marked increase is directly attributable to a much higher value of ν for ^{239}Pu and a much lower value of α. The results also indicate the beneficial aspects of threshold fissions in ^{238}U and ^{240}Pu. Reference 5 concludes that the results obtained provide tangible proof that a reactor fueled with ^{239}Pu can produce useful power and regenerate substantially more fuel than is consumed.

Resonance Absorption

In the case of isolated rods in the *NR-NR* approximation, collision theory yields

$$RI = \int \left[P_0 \frac{\sigma_p}{\sigma_0} + (1 - P_0) \right] \sigma_a \, dE/E$$

where σ_0, σ_a, and σ_p are the total, absorption, and potential scattering of the fuel, and P_0 is the nonescape probability from the fuel region. If the Wigner rational approximation is used, i.e.,

$$P_0 = \frac{x}{1 + x}$$

where x is the average optical chord length of the rod for a given energy, then the heterogeneous resonance integral is equivalent to the homogeneous resonance integral in which a new potential scattering is defined as

$$\sigma_p' = \sigma_p + \frac{\sigma_0}{x}$$

Reference 8 investigates the use of three better approximations to P_0 that are rational forms in x, namely:

1. From Booth,

$$P_0 = \frac{x(x + c)}{(x + b)^2}$$

2. From Carlvik and Fukai,

$$P_0 = \frac{2x}{x + 2} - \frac{x}{x + 3}$$

3. From Sauer,

$$P_0 = 1 - \frac{1}{x}\left[1 - \left(1 + \frac{x}{n+1}\right)^{-(n+1)}\right]$$

by comparison with the exact escape probabilities.

None of these methods can easily take into account differences in resonance parameters. Reference 9 considers the exact escape probability

$$P_0(x) = 1 - P_0(x) = \left[1 + \frac{x}{A(x)}\right]^{-1}$$

and obtains an average

$$\overline{A} = \frac{1}{I}\int_{-\infty}^{\infty} A\, dI$$

where I is the effective resonance integral for a particular resonance. Because the Doppler effect in each resonance is not proportional to its resonance integral, the use of the same relation for P_0 for a series of resonances in ^{238}U, for example, could lead to relatively large errors in temperature coefficients.

A form of the Dancoff factor based on cell calculations with white boundaries—i.e., all neutrons striking the cell boundary are returned with a cosine azimuthal distribution and do not follow the laws of specular reflection—is shown, in Ref. 8, to lead to results in good agreement with Monte Carlo calculations. The paper also justifies the use of the white-boundary condition on theoretical grounds.

Heterogeneous Graphite-Moderated Reactors

A design calculation method for gas-cooled graphite-moderated reactors has been coded in FORTRAN II in the ARGOSY program.[10] The principal approximations are:

1. Spatial effects in fuel and moderator are ignored, and mean fuel and mean moderator effects only are evaluated.

2. The generalized heavy-gas approximation is used to treat neutron thermalization.

3. Resonance integrals are not evaluated in the method but are obtained (in the case of ^{238}U) from tabular data.

Three energy groups with upper-energy cutoffs of 4 ev, 10 kev, and 10 Mev are used.

Thermal-Group Calculation

A three-region cylindrical cell, with fine structure within the fuel region reduced by simple flux-weighting factors, is used with about 100 energy points. An interpolation between narrow and wide resonance theory is used to compute fluxes through the plutonium resonance range. The thermalization in both fuel and moderator is approximated by the operator

$$L\phi = \xi\Sigma_s\, d/dx\{f(x)\,[x\phi'(x) + (x-1)\phi(x)]\} \qquad (x = E/kT)$$

where $f(x)$ is adjusted for crystal-binding effects as a function of plutonium concentration and moderator temperature. The coupled fuel and moderator equations are integrated using a finite-difference scheme.

Resonance-Group Calculation

Tabular values for the ^{238}U effective resonance integral as a function of fuel temperature and σ_{ex} are utilized.

$$\sigma_{ex} = \frac{\gamma S_{eff}}{4N_{238}\overline{V}_{fuel}}$$

where γ is a factor to correct for inaccuracies in the normal Wigner rational approximation and S_{eff} is the effective surface of the fuel element or cluster. These tables were made for uranium oxide and metal by considering for each resonance the proper mixture of narrow and wide resonance for potential scattering cross sections of uranium and oxygen. For ^{235}U and ^{239}Pu resonances, the infinite resonance integrals are reduced by factors allowing for self-shielding and shielding by ^{238}U and other isotopes. These can reduce the dilute values by about 20%. The spectrum in this group is not calculated, but effects of other absorbers are taken into account.

Fast-Group Calculation

A collision-probability approach is used in obtaining reaction rates in fuel and moderator for each of three energy subgroups where a spatially flat fission source in the fuel is assumed. This yields flux-weighted capture, fission, and removal cross sections. Diffusion coefficients for all groups are modified by streaming factors in the radial and axial directions.

Point core criticality can be achieved through changes in leakage, absorption, or fission source. Equivalent control-rod cross sections are evaluated by determining the extrapolation distance from blackness coefficients as a function of energy. A simple point burnup calculation can also be performed. The IBM-7090 time required for a complete calculation including burnup is about 5 min.

Reduced-Delayed-Neutron-Group Representation

In the analysis of the dynamic behavior of a reactor, considerable simplification results from the use of a reduced number of delayed-neutron groups, often with little sacrifice in accuracy. The selection of the reduced-group parameters (delayed-neutron yield and decay constant) generally depends on the type of transient being investigated. Reference 11 develops a reduced-group model chosen so that the resulting representation matches the reactor transfer function exactly in the limit of both very-low and very-high frequency. This requirement leads to the so-called "asymptotic" representation, the parameters for which are obtained from the following relations:

$$\sum_{j=1}^{m} \beta_j = \sum_{i=1}^{n} \beta_i \tag{1}$$

$$\sum_{j=1}^{m} \beta_j \lambda_j = \sum_{i=1}^{n} \beta_i \lambda_i \tag{2}$$

$$\sum_{j=1}^{m} \frac{\beta_j}{\lambda_j} = \sum_{i=1}^{n} \frac{\beta_i}{\lambda_i} \tag{3}$$

$$\sum_{j=1}^{m} \frac{\beta_j}{\lambda_j^2} = \sum_{i=1}^{n} \frac{\beta_i}{\lambda_i^2} \tag{4}$$

where β = delayed-neutron yield
λ = decay constant
i = group index of the physical-decay groups
n = number of the physical-decay groups
j = group index of the reduced groups
m = number of the reduced groups

Equations 1 and 2 result from matching the transfer function in the high-frequency limit, and Eqs. 3 and 4 result from matching the low-frequency limit. The equations as given hold for any number of reduced groups, but at least two groups must be used to satisfy all four conditions.

In some cases it is necessary to represent a particular group explicitly, for example, the longest lived group in cases where reactor shutdown is of interest or the shortest lived group for very rapid transients. In such a case the remaining groups are selected to satisfy Eqs. 1 to 4. Reference 12 contains a compilation of reduced-group parameters for various fissile isotopes with one reduced group (Eqs. 1 and 3), two groups (Eqs. 1 to 4), and three groups (Eqs. 1 to 4 with either the longest or shortest lived delay group represented explicitly).

Reference 13 reports a method of obtaining reduced-delay-group parameters by a least-squares fit. The parameters are chosen such that the integral

$$\int_{\omega} \left\{1 - \frac{\mathrm{Re}\,[F(j\omega)]}{\mathrm{Re}\,[G(j\omega)]}\right\}^2 d \ln \omega$$

is minimized where $G(j\omega)$ is the transfer function with all six delay groups and $F(j\omega)$ is the transfer function with the reduced groups. Results for two, three, and four reduced groups are tabulated for all fissile isotopes with the least-squares fit over a range of frequencies (ω) of 0.001 to 10 radians/sec. A comparison of the reduced-group parameters obtained from the asymptopic and the least-squares approach as determined in Ref. 13 is given in Table I-1. In addition, Ref. 13 compares calculations of both the reactor transfer function and the reactor response to positive- and negative-

reactivity steps with the reduced-group models and the full six-delay-group model.

Table I-1 COMPARISON OF REDUCED-DELAYED-NEUTRON-GROUP PARAMETERS FOR ^{235}U (THERMAL FISSION)[13]

	Asymptotic	Least squares
Two groups		
λ_1	0.0252	0.0410
λ_2	0.566	0.540
β_1	0.00194	0.00293
β_2	0.00459	0.00360
Three groups (longest lived group isolated)		
λ_1	0.0124	0.0124 (0.0278)*
λ_2	0.0342	0.0512 (0.0231)
λ_3	0.609	0.590 (1.568)
β_1	0.00022	0.00022 (0.00185)
β_2	0.00263	0.00299 (0.00364)
β_3	0.00367	0.00332 (0.00104)

*Three-groups straight least-squares fit.

References

1. E. A. Moore and C. L. Peckinpaugh, On-Line Shim Rod Calibration, USAEC Report NAA-SR-9511, Atomics International, Aug. 1, 1964.
2. M. R. Pellet, Core II Physics Tests on the Sodium Reactor Experiment, USAEC Report NAA-SR-9510, Atomics International, Aug. 1, 1964.
3. V.W. Gustafson, Plutonium Recycle Test Reactor Power Test Results, USAEC Report HW-80253, Hanford Atomic Products Operation, December 1963.
4. J. F. Perkins and R. W. King, Energy Release from the Decay of Fission Products, *Nucl. Sci. Eng.*, 3(6): 726-746 (June 1958).
5. R. R. Smith, R. O. Haroldsen, and F. D. McGinnis, Stability Considerations for a Plutonium Loading in EBR-I, USAEC Report ANL-6863, Argonne National Laboratory, May 1964.
6. R. R. Smith, R. O. Haroldsen, R. E. Horne, and R. G. Matlock, The Breeding Ratio of a Plutonium Loading in EBR-I, USAEC Report ANL-6789, Argonne National Laboratory, February 1964.
7. P. Kafalas et al., Determination of the Ratio of Capture to Fission Cross Sections in EBR-I, *Nucl. Sci. Eng.*, 2(5): 657 (September 1957).
8. D. C. Leslie, J. G. Hill, and A. Jonsson, Improvement to the Theory of Resonance Escape in Heterogeneous Fuel. 1. Regular Arrays of Fuel Rods, British Report AEEW-R-353, 1964.
9. J. M. Otter, Escape Probability Approximations in Lumped Resonance Absorbers, USAEC Report NAA-SR-9744, Atomics International, August 1964.
10. J. G. Tyror, A Method of Lattice Calculation for Gas-Cooled Graphite-Moderated Reactors, British TRG-Report-754(W), 1964.
11. R. E. Skinner and E. R. Cohen, Reduced Delayed Neutron Group Representations, *Nucl. Sci. Eng.*, 5(5): 291-298 (May 1959).
12. R. W. Albrecht and C. Metelmann, The Use of Reduced Delayed Neutron Group Representations in Nuclear Reactor Simulation, USAEC Report HW-81076, Hanford Atomic Products Operations, March 1964.
13. T. E. Springer, Delayed Neutron Reduced Groups by Least Squares, USAEC Report LA-3082, Los Alamos Scientific Laboratory, December 1961.

Section

II

Power Reactor Technology

Fluid and Thermal Technology

Liquid Metals

References 1 and 2 are literature reviews of the engineering properties of various liquid metals. They contain data on properties such as density, thermal conductivity, electrical resistivity, specific heat, surface tension, vapor pressure, and viscosity for metals such as mercury, sodium, sodium-potassium, potassium, rubidium, and lithium. Reference 1 is directed specifically to liquid-metal heat transfer by forced convection and presents a comparison of theoretical and experimental results. The report presents "recommended" equations suitable for the engineering calculation of heat transfer in fully developed turbulent flow in circular tubes, heat transfer in fully developed turbulent flow through tubes of noncircular cross section, and heat-transfer-coefficient correlations for flow parallel to bundles of circular rods and across a staggered tube bank. The discrepancies between experimental and theoretical results are discussed, and several reasons for the discrepancies are suggested.

Data on forced-convection heat transfer and pressure drop for boiling potassium are given in Ref. 3. The particular system considered in the reference is quite specialized in that the experiments were done to obtain design data for a potassium boiler constructed of serpentine tubes. Nevertheless, the reference gives insight into the difficulties of experimentation with liquid metals and the techniques employed to determine heat-transfer coefficients in rather complex systems. Figure II-1 illustrates the forced-convection local-boiling heat-transfer coefficients for potassium boiling inside serpentine tubes. The figure shows the "best-fit" correlation. The data, which show considerable scatter, are not reproduced here, but are given in Ref. 3. The range of experimental parameters is shown in Table II-1.

It is interesting to note that the stability of the boiling loop proved to be a continuing problem in the experiments. The loop, which was constructed of Haynes 25 alloy, consisted of a preheater, a test boiler, a superheater, and an air-cooled condenser, coupled with an electromagnetic flowmeter and pump. Much of the instability problem was said to originate in the preheater-preboiler portion of the loop as the result of subcooled nucleate boiling, despite the fact that a rather large pressure drop was established by use of a throttle valve just downstream of the electromagnetic pump. The authors conclude that the stability of two-phase

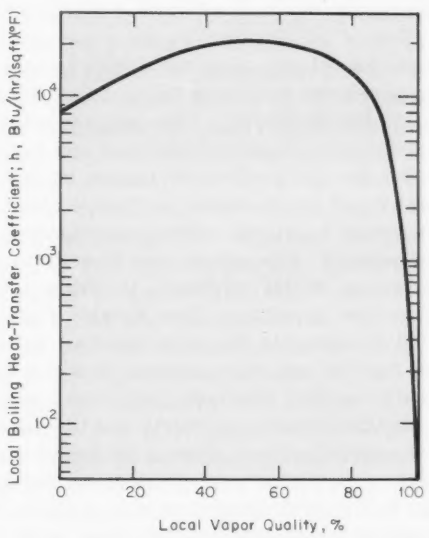

Fig. II-1 Forced-convection local-boiling heat-transfer coefficients for potassium inside a serpentine tube.[3]

Table II-1 RANGE OF EXPERIMENTAL PARAMETERS IN BOILING POTASSIUM EXPERIMENT[3]

Potassium flow rate, lb/hr	17 to 25
Vapor quality, %	0 to 100
Boiling ΔT, °F	2 to 170
Boiling temperature, °F	1625 to 1725
Heat flux in test boiler, Btu/(hr)(sq ft)	17,000 to 52,000
Max. heat flux in preboiler	64,000
Boiling pressure, psia	42 to 62
Max. vapor velocity, ft/sec	330
Test duration, hr	3625
Boiling hours	980

potassium systems cannot be studied by simulation with water or other common fluids. The pressure-drop data taken during the experiments were found to correlate within ±20% by the Lockhart-Martinelli correlation.

Reference 4 presents data on the boiling-heat-transfer coefficients and burnout heat fluxes for pool boiling of sodium. The reference describes in some detail two sodium loops, the larger of which accommodates an instrumented electric heating element on which accurate surface-temperature measurements can be made at heat fluxes up to 10^6 Btu/(hr)(sq ft) in boiling sodium. The test-section portion of this large loop, called the "working loop" in Ref. 4, is fabricated of graphite, electrically insulated with a boron nitride sleeve. The test section, which is heated by the resistance of the graphite, is capable of working to the heat flux of 10^6 Btu/(hr)(sq ft); a second test section heated by electron bombardment is being developed to extend the heat flux limit to 5×10^6 Btu/(hr)(sq ft). The data recorded in Ref. 4 on heat-transfer coefficients and burnout heat flux are of a preliminary nature but nevertheless would be of interest to the specialist.

Reference 5 reports on the determination of void fractions, slip ratios, and flow rates for liquid-vapor metal systems in pipes under critical-flow conditions. The Fauske model is applied to calculate the void fraction, the slip ratio, and the two-phase critical flow rates for mercury, cesium, rubidium, potassium, sodium, and lithium under the postulate that the mechanisms causing critical flow in the liquid-vapor systems are the same as in steam-water systems. Figure II-2 illustrates, for example, the theoretical prediction of the slip ratio for rubidium under critical-flow conditions. According to Ref. 5, no experimental data exist pertinent to the critical flow of liquid metals; it is therefore not possible to compare the theoretical predictions with experimental results.

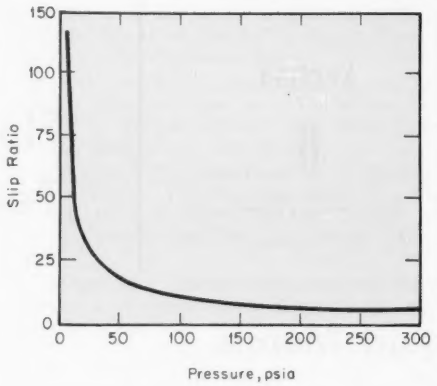

Fig. II-2 Theoretical prediction of slip ratio for rubidium under critical-flow conditions.[5]

Two-Phase Systems

The relatively large volume of literature pertinent to two-phase flow indicates continued interest in the associated phenomena. Reference 6 is an extensive annotated bibliography on the heat transfer and hydraulics of gas-liquid systems. A total of 2843 documents are cited in the bibliography, and the subjects covered represent a wide range of interests. These include such items as the critical heat flux, flow patterns, nozzles, phase and velocity distribution, pressure drops, separation of mixtures, transients and instability, turbulent flow, and visual observations. The references were published between 1950 and 1962 in *Nuclear Science Abstracts, Chemical Abstracts, Science Abstracts — Section A, Engineering Index,* and *Applied Mechanics Reviews.* It is believed that the volume will prove to be a valuable asset to workers in the field of two-phase hydraulics and heat transfer.

References 7 to 12 are somewhat specialized and will not be reviewed in detail. The consideration of the group as a whole, however, indicates the basic lines of attack in attempts to discover basic information on two-phase flow and heat transfer. References 7 and 8 deal with pool boiling. References 9 and 10 are air-water studies pertaining to annular, two-phase flow. References 11 and 12 deal with flow regimes. Reference 12 is particularly interesting in that it reports on an experimental program to determine the transition point between slug- and annular-flow regimes at elevated pressures.

The Armadilla loop at Argonne National Laboratory was used to produce a steam-water mixture at pressures up to 600 psig. Conductivity measurements were made in the riser of the test loop by means of a suitably designed probe. This probe measured the electrical resistance between the center of the pipe and the wall; when the probe was dry, the resistance was very high, and, when wet, the resistance was relatively lower. Figure II-3 is indicative of the results obtained in the study. The figure shows the superficial vapor velocity plotted against the superficial liquid velocity and indicates that the transition between the slug- and annular-flow regimes was not a step change, but that there existed a region designated as "transition" wherein the major mode of liquid transport corresponded to slugs with a large number of bubbles entrained in them. As the superficial vapor velocity was further increased, fully developed annular flow was established. It was found that the transition between the slug- and annular-flow regimes at a given pressure occurred at almost constant quality, independent of flow range, provided that the following relation was satisfied:

$$\frac{V_{gs}^2 \rho_g}{gD \rho_f} \geq 2.0$$

where V_{gs} is the superficial vapor velocity, D is the pipe diameter, and ρ_f and ρ_g are the liquid and vapor densities, respectively. The quality at which the transition occurred ranged from 8.6% at 215 psia to about 18% at 615 psia. The following quotation serves to summarize the results:[12]

> ... Physically, the picture that emerges from these experiments is as follows. When the quality is passed through at which slugs can form, they do. As the annular flow region is approached, these slugs begin to lose liquid to the wall as they rise, ultimately being completely consumed if the pipe is long enough.... If the heat flux were higher, or perhaps if the region in which slug flow could exist were shorter, slug flow might never develop, and one could go right from bubbly to annular flow.
>
> Repeated attempts to obtain bubbly flow in this apparatus always were unsuccessful. Either the heat flux was too low or the pump too small for this condition ever to exist. In the 0.875-in. ID pipe, the maximum inlet liquid velocity was only 10 ft/sec. This is apparently insufficient to give bubbly flow as the fully developed condition. In addition, the water was very pure, which also made it difficult to obtain bubbly flow. It would appear that bubbly flow is an important flow regime only when the pressure and/or the heat flux is very high.

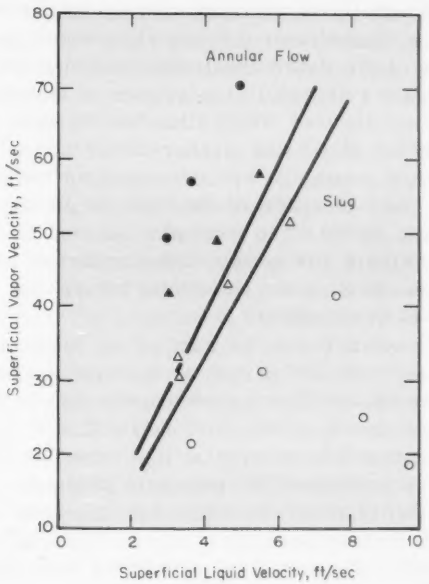

Fig. II-3 Flow-regime map for 0.375-in. pipe.[12] Pressure is 615 psia. (The open symbols are slug flow, and the solid symbols are annular flow.)

It is natural that both the analyst and the experimenter would like to "see" what is going on within the test section; indeed, the author of Ref. 12 does present pictures of air-water flow tests at low pressure. References 13 to 15 are devoted to results of photography and X radiography of two-phase flow systems. A perusal of these documents indicates that the problems in optics connected with photographing gas-liquid mixtures probably are as formidable as the problems of analyzing the results obtained from such experiments. The technique discussed in Ref. 14, that of radiography, appears quite promising in that it does allow studies using opaque tubing and high pressures. The discussion in that reference is devoted to a large extent to the mechanics of obtaining the X-ray photographs, although a few results of the experiments are given pictorially. The positive prints of the X-ray plates shown illustrate that it is remarkably easy to tell the positions of the liquid and gas phases (in this case air) within the tube, and the pictures show various flow regimes.

Reference 15 reports on experiments designed to study boiling flow of steam-water mixtures at atmospheric pressures. High-speed motion pictures were made for a variety of flow rates

and heat fluxes utilizing a transparent rectangular channel heated by a strip of metal at one side of the flow channel. The reference reproduces a relatively large number of frames of motion pictures which illustrate bubble-, coalescing slug-, and annular-flow regimes. An unusual procedure was developed for measuring the velocities of the various liquid and vapor phases. The reference also contains a quantitative discussion of the important variables affecting the transitions between the different flow regimes.

A relatively large number of publications (Refs. 16 to 23) pertain to the hydrodynamics of two-phase flow. Included are papers on two-phase pressure drop,[16,17] nozzle flow,[18,19] and the prediction of critical flow rates for two-phase mixtures.[20–23] Reference 16 compares a number of analytical methods for the prediction of two-phase pressure drop with experimental results. The analytical techniques were those of Levy, Marchaterre, and Martinelli and Nelson. Experimental pressure drops were measured for circular and annular channels. The results are compared graphically, and no single correlation was found to represent the data adequately. Neither the Martinelli and Nelson nor the Levy correlation provides for the effect of the mass flow on the pressure drop, and this effect appeared to be a relatively large one in the experimental results.

The information in Ref. 17 includes two-phase pressure-drop data as experimentally determined for a variety of piping components such as bends, tees, expansions, contractions, and valves. Most of the data were obtained at 1200 psia (although a few points were run at 800 and 1600 psia) at mass velocities from 1 to 4 million lb/(hr)(sq ft) and at qualities up to 24 wt.%. Pressure-drop ratios were determined for straight-pipe flow and were found to be correlated "favorably" by the Levy model. The effect of flow rate on the pressure-drop ratios was negligible, and the author mentions that this behavior is not consistent with the results of other investigators. The author[17] suggests that this comes about because of the relatively large pipe diameter — 2 in. — used in his measurements. The reference presents a correlation relating the two- to single-phase pressure-drop ratio of bends to the ratio for straight pipes over the pressure range 800 to 1600 psia. Resistance coefficients were obtained for contraction and expansion losses on the assumption of a homogeneous mixture, and the coefficients agreed reasonably well with the data presented in standard engineering textbooks. The ratio of the two- to single-phase pressure drop for flow through an orifice at 1200 psia was calculated by the homogeneous model, and the results appeared to agree fairly well with the experimental data. The pressure losses in flows through gate and globe valves, however, did not correlate very well with calculations based on the homogeneous model.

The expansion of two-phase fluids through converging-diverging nozzles is discussed in Refs. 18 and 19. The emphasis in these two papers is not on reactor design, although the information they present could be applied to mass-flow-rate determination. References 20 to 23 pertain to the predictions of critical flow of single- and two-phase mixtures. These references contain both experimental and analytical predictions of critical flow rates in a variety of geometries; the results may be useful in the field of nuclear safety, since two-phase critical flow usually would occur in the discharge of coolant from a pipe or pressure-vessel break into the reactor containment system. Reference 21, for example, reports on experimental determination of the discharge of steam-water mixtures from short lengths of pipe at upstream pressures approaching 2000 psia. The reference[21] presents an equation correlating experimentally determined data.

The subject of boiling burnout is covered in Refs. 24 to 27. Reference 24 gives the results of an investigation into forced-convection burnout in Freon and deals with the uniformly heated round tubes utilizing vertical upflow. The use of Freon (also called "Acton" in the reference) is an attempt to gain an insight into the mechanism and important parameters affecting burnout in steam-water systems without encountering the many experimental difficulties involved with the actual use of steam and water. The material (Freon-12) has low vapor pressure and a low latent heat. This combination of physical properties enabled the Freon loop to operate at low pressures and temperatures with low power requirements. The reference reports experimental data and compares them to results obtained in steam-water experiments, with the following conclusions:[24]

> The qualitative similarity in shapes of functions and detailed effects between the Acton 12 data at 155 pounds per square inch and data for water at

1000 pounds per square inch indicates a high probability of success in developing model techniques at least for the study of burn-out in high-pressure water systems.

References 25 to 27 all deal with experimental studies of burnout in bundles of heated rods. This subject was previously considered in the Spring 1964 issue of *Power Reactor Technology*, 7(2): 154-165. This previous review concluded that the experimental results for burnout in multirod geometry were not well understood. Part of the problem was believed to lie in the difficulty of determining the amount of mixing from one flow subchannel to another within the multirod bundle. Accordingly the information appearing in Ref. 25 is of interest in that it reports boiling burnout data taken with two different types of rod spacers, "wires" and "warts." The Hanford tests done with the wire-wrapped bundle were reviewed in the earlier issue of *Power Reactor Technology*, and the data given in Ref. 25 compare results obtained when the wire wrapping on the rods is replaced by the so-called warts. The warts were made of alumina having a length of $^{9}/_{16}$ in., a width of 0.17 in., and a thickness of 0.048 in. and were positioned on the heated rods by placing them in slots cut in Inconel ferrules soldered to the heated rods. The test section was housed in a horizontal 3.25-in.-ID pressure tube, and pressure was controlled to 1200 psig. Results indicated that "there is no discernible difference in the burnout heat fluxes between the test sections with rods spaced with wire wraps and the test sections with rods spaced with warts."[25] The authors comment[25] that this was somewhat unexpected, in that they believed that the degree of mixing would be increased by the use of the wire-wrapped test section and that this increase would result in higher burnout heat fluxes. A number of explanations offered for the lack of difference in the two sets of data include the following: (1) the amount of mixing between the subchannels is the same with the wire wrap as with the warts; (2) a spacing effect predominates over mixing in determining the burnout conditions; (3) the increased mixing caused by the wires is offset by the tendency of the wires to strip the liquid film from the rods.

Reference 26 reports on burnout experiments employing a 19-rod bundle as a test section and using "fog" as a coolant. A cross section of the bundle is shown in Fig. III-1 of *Power Reactor Technology*, 7(2): 154. The test section used to take the data in Ref. 26 employed the wart type spacers to ensure that the rod-to-rod spacing (0.074 in.) was maintained. Experiments were conducted at pressures of 1000 and 1200 psia with flow rates from 500,000 to 2 million lb/(hr)(sq ft). One of the test sections had a "flow diverter" present (about 14 in. upstream of the heated length) which was designed to direct the coolant flow to the interior of the bundle at that point; the second test section was similar but was constructed without the presence of the flow diverter. The presence of the flow diverter had little effect on the burnout heat flux when the coolant at the inlet was fog, but the diverter did increase the value of the burnout heat flux some 10 to 20% for subcooled water. Possibly the most important piece of information coming from the tests[26] was the demonstration of the importance of the hydraulic stiffness of the system on the value of the burnout heat flux. Figure II-4 illustrates the burnout heat flux as a function of the outlet enthalpy for a pressure of 1200 psia. The discontinuities in the curves shown in Fig. II-4 were believed to be caused by the presence of a compressible medium, steam, in that portion of the test loop between the steam generator and the test section. The presence of this instability complicates the data and makes their comparison to other results difficult. Of more importance, it indicates extreme care must be taken in applying laboratory data to reactors whose hydraulic characteristics may be different from those of the laboratory apparatus.

In British work[27] on the effect of rod spacing on burnout in a simulated rod bundle, the test section simulated the gap between the rod type

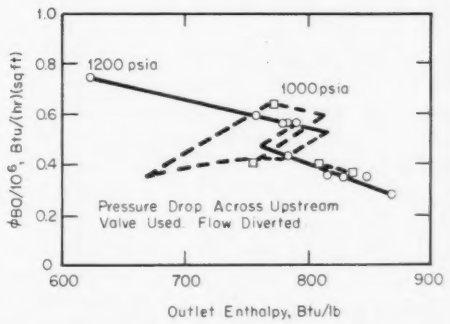

Fig. II-4 Effect of system pressure on boiling burnout for 19-rod bundles at a flow rate[26] of 500,000 lb/(hr)(sq ft).

elements in a multirod bundle by means of a "dumbbell" test section. The cross section of the dumbbell test section is shown in Fig. II-5; the use of such a mock-up permits experiments to be carried out in loops of reduced power capability. The heat generation at the

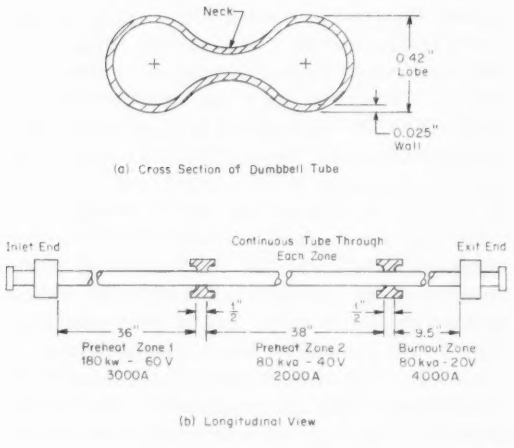

Fig. II-5 Details of the dumbbell test section.[27]

neck of the dumbbell test section was increased for some of the runs by fixing a strip of stainless steel to each neck, and tests were run at a pressure of 960 psia, with a mass velocity of 2 million lb/(hr)(sq ft) and vertical upflow of water. Tests were also made with a tubular test section of the same diameter as the lobe of the dumbbell test section. The total length of the test section was about 7 ft, with the first 6 ft being utilized as a preheater and the last 9.5 in. being instrumented to detect burnout. The surfaces of the neck portion of the test section could be forced closer together by insulating blocks, and the gap therein varied from about 0.04 to 0.2 in. The results indicated that for tests with uniform peripheral heat flux the value of the gap was unimportant for gaps ranging within the values just mentioned. Burnout occurred at the exit end of the test section and on the lobe rather than at the neck. Additional tests were done with local increases of heat flux at the neck of the test section, and an arbitrary increase of 40% in heat flux was made by the inclusion of the metal strips. The effect of the gap was again small, although in these runs burnouts did take place in the region of the test-section neck. Correlation of the tubular burnout data[27] with the data from the dumbbell illustrated that burnout occurred in the two test sections at equivalent values of heat flux.

The remaining group of reports[28–32] deals with experimental and analytical studies of the dynamics of two-phase systems. Three of the reports[28–30] cover analytical studies, and the remaining two reports discuss experimental results. The analytical approaches are all based on the fundamental conservation equations dealing with mass, energy, and momentum plus an equation of state. They are different in the techniques used to solve the equations and the models of the system upon which the equations are based. The treatment in Ref. 28, for example, uses the simplified model illustrated in Fig. II-6, and the differential equations are solved by the "modified-Euler" integration process combined with appropriate iterative procedures. The author of Ref. 29 considers the idealized natural-circulation system shown in Fig. II-7, and the solution of the equations is accompanied by perturbation theory. Figure II-8 illustrates the system studied in Ref 30, in which perturbation theory is again used to achieve a solution. The treatment in Ref. 28 is quite complete; reactivity feedback in the reactor is provided and is coupled into the time-dependent solutions. Separate energy-conservation equations for the fuel, cladding, and the heat exchanger are also included, and separated flow is assumed. The author of Ref. 29 obtains the void-reactivity feedback by integrating the product of the perturbed void fraction, both spatially

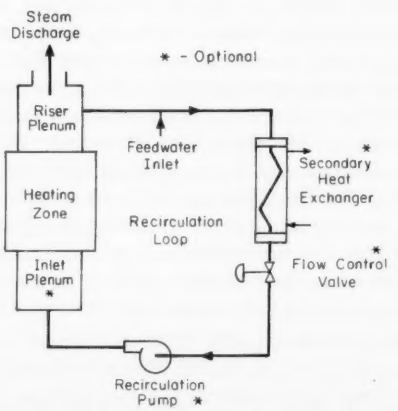

Fig. II-6 Idealized boiling-water system.[28]

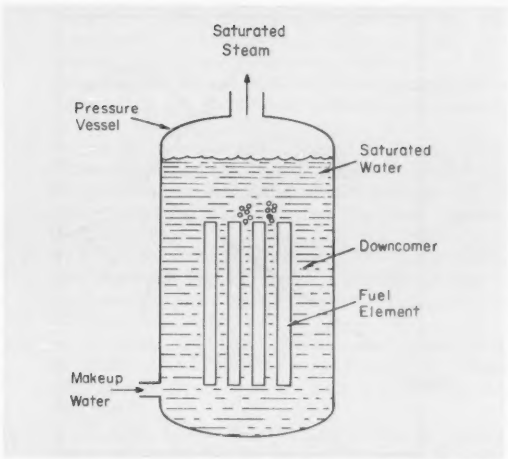

Fig. II-7 Model of a natural-circulation boiling-water reactor.[29]

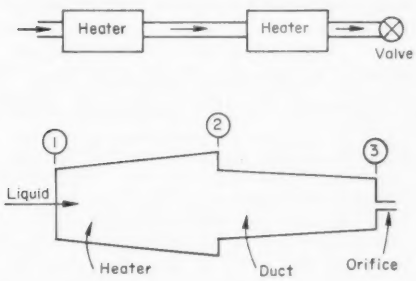

Fig. II-8 Configuration of system studied in Ref. 30.

and temporally, and the reactivity worth of the voids. The treatment of power generation in Ref. 30 assumes that the rate of vapor generation in the heater is constant or is proportional to the system density at point 2 (see Fig. II-8).

It is feasible here only to mention a few of the general results of the rather complex dynamic analyses. The mathematical model developed in Ref. 28 is compared to experimental results obtained at General Electric Company, Atomic Power Equipment Department. The authors conclude that "the period of oscillations and threshold of instability predicted by the present analysis are in good agreement with the test results." The analyses are then applied in studying the response of a "typical" boiling-water reactor to a variety of perturbations. In Ref. 29 the analytical solutions obtained are applied to several specific problems, namely, the dependence of stability on steady-state conditions, the effect of pressure drops in the downcomer and at the inlet to the channel, and the stability of a parallel-channel system with a common downcomer. The effect of the channel length on the dynamic behavior of the system is also studied.[29] The author of Ref. 30 has specialized his solution to the case of a short heater followed by a long insulated duct and orifice, and also a long heater immediately followed by an orifice with no insulated duct. Briefly the author concludes that, whenever a fluid density ratio greater than about 3 exists across an evaporator, there is a possibility of the development of flow oscillations.

The experiments reported in Ref. 31 are preliminary in nature and were done with two parallel heated channels. Both single-phase liquid (subcooled water) at atmospheric pressure and steam-water mixtures were employed as feed to the test sections. Heating was accomplished by the condensation of steam at pressures ranging from 20 to 50 psi. The results illustrate that a negative slope of the curve of mass flow rate vs. pressure is not a necessary condition for the occurrence of oscillatory instabilities. The authors also conclude that, when there is net quality in the feed to the heated test section, no oscillatory instabilities will occur. This conclusion appears to disagree with the data presented in Ref. 26; in that study the presence of steam in the piping between the steam generator and the test section was believed to have allowed flow oscillations in the test section. The problem is complicated, however, by the fact that the "springiness" of the entire test loop depends on its constructional details; and, although the test loop used to take the data appearing in Ref. 31 did employ two-phase mixtures at the test-section inlet, it may well be that the flow loop nevertheless was "stiff."

The test section utilized in Ref. 32 was an electrically heated stainless-steel tube (0.045 in. in inside diameter and 4.5 in. long). Although the tests were run at 200 psia, a pressure lower than that ordinarily used for water type reactors, the results still are of general interest. The author notes that at low values of subcooling it is possible to obtain high void fractions due to the presence of unquenched bubbles. The bubbles exist because, as the subcooling of zero is approached, the temperature driving force

transferring heat from the bubbles to the bulk liquid becomes small, with the result that the bubbles have relatively long lifetimes. The presence of the nonequilibrium situation within the flow channel resulted in a departure from the characteristic burnout pattern in subcooled water. The most noticeable result of this was the reduction of the burnout heat flux to relatively low values. The author suggests that this is due to the initiation of "froth flow" as the unquenched bubbles are entrained in the liquid. The reference presents a table of critical-heat-flux data taken with the apparatus, and each burnout point is accompanied by a description of a hypothesized local flow regime. The local flow regimes were identified by consideration of the behavior of the test-section instrumentation and the past history of a particular run. Some idea of the technique can be obtained by considering Fig. II-9. Figure II-10 illustrates the effect of instabilities on the burnout heat flux for the hypothesized annular flow. The author comments on the figure as follows:

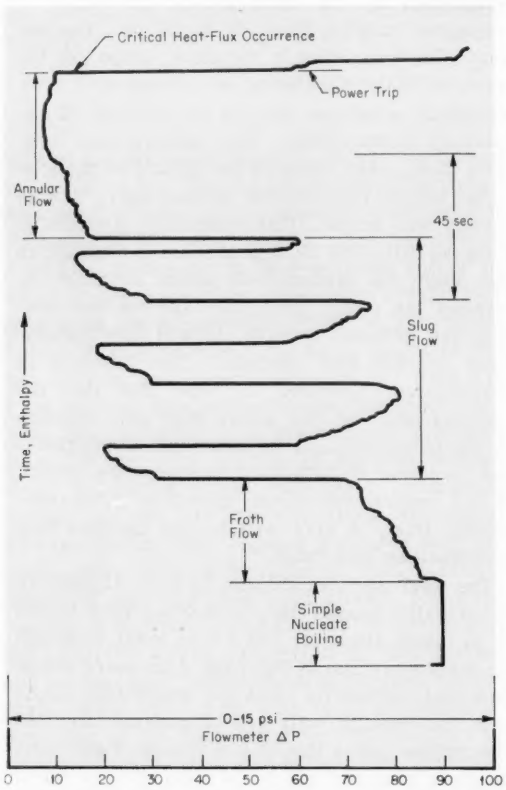

Fig. II-9 Froth flow, periodic vapor slugging, and stable annular flow during net steam generation.[32]

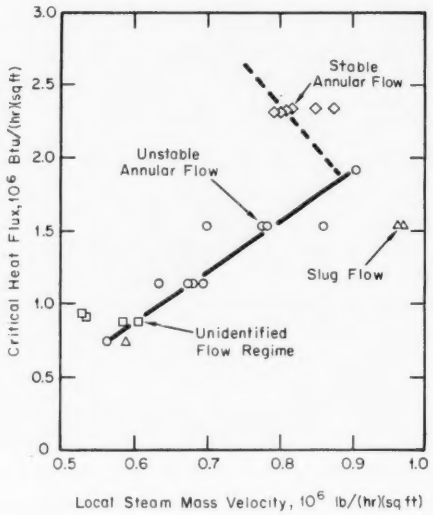

Fig. II-10 Effect of flow regime and degree of hydrodynamic instability upon critical-heat-flux occurrence during net steam generation[32] *at 200 psia.*

> The positive slope of the critical heat flux-steam mass velocity relationship [see Fig. II-10] which is characteristic of unstable annular flow, is directly counter to the negative slope typical for stable flow. Since the slug-flow data follow a similar behavior, this characteristic may be applied to distinguish between stable and unstable flow conditions in systems using high-damping, slow-response secondary flow meters, such as mercury manometers.

This was one of the points made in the review article in the Fall 1964 issue of *Power Reactor Technology*, 7(4): 335.

References

1. R. Herrick, Liquid Metal Heat Transfer by Forced Convection, British TRG-Report-546, July 2, 1963.
2. G. F. Burdi, Snap Technology Handbook, Volume I. Liquid Metals, USAEC Report NAA-SR-8617 (Vol. I), Atomics International, Aug. 1, 1964.
3. E. Bernstein, J. P. Petrek, G. J. Rose, and J. J. Horan, Experimental Results of Forced Convection Boiling Potassium Heat Transfer and Pressure Drop Tests, USAEC Report PWAC-429, Pratt & Whitney Aircraft Division, United Aircraft Corp., July 16, 1964.
4. R. C. Noyes, Boiling Studies for Sodium Reactor Safety. Part I. Experimental Apparatus and Results of Initial Tests and Analysis, USAEC Report NAA-SR-7909, Atomics International, Aug. 30, 1963.

5. Hans K. Fauske, Two-Phase Critical Flow with Application to Liquid-Metal Systems (Mercury, Cesium, Rubidium, Potassium, Sodium, and Lithium), USAEC Report ANL-6779, Argonne National Laboratory and Associated Midwest Universities, October 1963.
6. Robert R. Kepple and Thomas V. Tung, Two-Phase (Gas-Liquid) System: Heat Transfer and Hydraulics, An Annotated Bibliography, USAEC Report ANL-6734, Argonne National Laboratory, July 1963.
7. W. R. Beasant and H. W. Jones, The Critical Heat Flux in Pool Boiling Under Combined Effect of High Acceleration and Pressure, British Report AEEW-R-275, July 1963.
8. W. L. Owens, Jr., An Analytical and Experimental Study of Pool Boiling with Particular Reference to Additives, British Report AEEW-R-180, May 1963.
9. L. E. Gill, G. F. Hewitt, and P. M. C. Lacey, Sampling Probe Studies of the Gas Core in Annular Two-Phase Flow: Part II. Studies of the Effect of Phase Flow Rates on Phase and Velocity Distribution, British Report AERE-R-3955, June 1963.
10. G. F. Hewitt and P. M. C. Lacey, The Breakdown of the Liquid Film in Annular Two-Phase Flow, British Report AERE-R-4303, August 1963.
11. A. A. Kudirka, Two-Phase Heat Transfer with Gas Injection Through a Porous Boundary Surface, USAEC Report ANL-6862, Argonne National Laboratory, March 1964.
12. Peter Griffith, The Slug-Annular Flow Regime Transition at Elevated Pressure, USAEC Report ANL-6796, Argonne National Laboratory, November 1963.
13. K. D. Cooper, G. F. Hewitt, and B. Pinchin, Photography of Two-Phase Flow, British Report AERE-R-4301, May 1963.
14. R. T. P. Derbyshire, G. F. Hewitt, and B. Nicholls, X-Radiography of Two-Phase Gas-Liquid Flow, British Report AERE-M-1321, January 1964.
15. John H. Vohr, A Photographic Study of Boiling Flow, USAEC Report NYO-9650, Columbia University, Oct. 25, 1963.
16. M. Muscettola, Two-Phase Pressure Drop—Comparison of the "Momentum Exchange Model" and Martinelli and Nelson's Correlation with Experimental Measurements, British Report AEEW-R-284, May 1963.
17. D. E. Fitzsimmons, Two-Phase Pressure Drop in Piping Components, USAEC Report HW-80970 (Rev. 1), Hanford Atomic Products Operation, Mar. 20, 1964.
18. E. S. Starkman, V. E. Schrock, K. F. Neusen, and D. J. Maneely, Expansion of a Very Low Quality Two-Phase Fluid Through a Convergent-Divergent Nozzle, *J. Basic Eng.*, 86: 247-256 (June 1964).
19. Joseph A. Vogrin, Jr., An Experimental Investigation of Two-Phase, Two-Component Flow in a Horizontal, Converging-Diverging Nozzle, USAEC Report ANL-6754, Argonne National Laboratory, July 1963.
20. K. Goldmann, R. Hankel, and R. P. Stein, An Equation for the Critical Mass Velocity of Homogeneous Vapor-Liquid Mixtures at Low Pressures, *J. Appl. Mech.*, 31(3): 380-382 (September 1964).
21. F. R. Zaloudek, Steam-Water Critical Flow from High Pressure Systems. Interim Report, USAEC Report HW-80535, Hanford Atomic Products Operation, January 1964.
22. F. R. Zaloudek, The Critical Flow of Hot Water Through Short Tubes, USAEC Report HW-77594, Hanford Atomic Products Operation, May 1963.
23. S. Levy, Prediction of Two-Phase Critical Flow Rate, *J. Heat Transfer*, 87(1): 53-58 (February 1965).
24. G. F. Stevens, D. F. Elliott, and R. W. Wood, An Experimental Investigation into Forced Convection Burn-Out in Freon, with Reference to Burn-Out in Water. Uniformly Heated Round Tubes with Vertical Up-Flow, British Report AEEW-R-321, January 1964.
25. J. M. Batch and G. M. Hesson, Comparison of Boiling Burnout Data for 19-Rod Bundle Fuel Elements Spaced with "Wires" and "Warts," USAEC Report HW-80391 (Rev. 1), Hanford Atomic Products Operation, Jan. 15, 1964.
26. G. M. Hesson, D. E. Fitzsimmons, and J. M. Batch, Boiling Burnout Experiments with Fog-Cooled Nineteen-Rod Bundle Test Sections, USAEC Report HW-80523 (Rev. 1), Hanford Atomic Products Operation, March 1964.
27. D. H. Lee and R. B. Little, U. K. Atomic Energy Authority. (Unpublished)
28. A. N. Nahavandi and R. F. von Hollen, A Space-Dependent Dynamic Analysis of Boiling Water Reactor Systems, *Nucl. Sci. Eng.*, 20(4): 392-413 (December 1964).
29. Chathilingath K. Sanathanan, Dynamic Analysis of Coolant Circulation in Boiling Water Nuclear Reactors, USAEC Report ANL-6847, Argonne National Laboratory, April 1964.
30. A. H. Stenning, Instabilities in the Flow of a Boiling Liquid, *J. Basic Eng.*, 86: 213-217 (June 1964).
31. D. J. Pulling and J. G. Collier, Instabilities in Two-Phase Flow. Preliminary Experiments, British Report AERE-M-1105, July 1963.
32. R. J. Weatherhead, Heat Transfer, Flow Instability, and Critical Heat Flux for Water in a Small Tube at 200 psia, USAEC Report ANL-6715, Argonne National Laboratory, June 1963.

Section

III

Power Reactor Technology

Fuel Elements

Fuel-Performance Evaluations

An engineering proof test of seven UO_2 fuel rods, which were 0.412 in. in diameter and which were clad with type 304 stainless steel, was successfully completed[1] in a borated pressurized-water loop in the Westinghouse Testing Reactor (WTR). The loop conditions[1] are summarized below:

Average coolant inlet temperature, °F	560 to 580
Coolant pressure, psi	2000
Flow rate, gal/min	62
Chlorine, ppm	<0.1
Boron (as H_3BO_3), ppm	1500 ± 50
Hydrogen, cm^3 (STP) per kilogram of H_2O	30
Oxygen, ppm	<0.1

The elements were irradiated to a maximum burnup of 4000 Mwd per metric ton of uranium at a maximum heat flux of 340,000 Btu/(hr)(sq ft) for the purposes of demonstrating the feasibility of boron chemical shim and the performance of fuel rods in the large-plant design of the Large Closed Cycle Water Reactor Research and Development (LRD) Program.* The fuel bundle was fabricated as a simulation of a four-rod segment of the fuel assembly in the large plant. The 2.07% enriched UO_2 fuel pellets, of 0.379-in. diameter, were fabricated to 96% of the theoretical density and were clad with 10% cold-worked type 304 stainless steel that was 0.016 in. thick. The fuel-cladding diametral gap of 0.004 in. was filled with air. An attempt to measure in-pile thermal expansion of the UO_2 fuel column by means of markers inside the cladding, to differentiate between the performance of dished and flat pellets, did not succeed. Postirradiation evaluation indicated satisfactory performance, and the results of fission-gas-release measurements and postirradiation microstructure evaluations were consistent with those generally anticipated for UO_2 fuel rods operating under comparable conditions.

The rods that achieved an average burnup of 6.4×10^{20} fissions/cm^3 in the blanket of the Shippingport reactor at the end of the third seed life have been examined.[2] One of these rods operated at an average cladding-surface temperature of 515°F and a lifetime average surface heat flux of 155,000 Btu/(hr)(sq ft). Although the lifetime average heat flux of 139,000 Btu/(hr)(sq ft) noted for the second rod would appear to provide little additional interest, it was found that a heat flux of 428,000 Btu/(hr)(sq ft) had occurred in this rod for about 200 equivalent full-power hours.

Results of postirradiation examinations indicated no cladding failures, no changes in fuel-rod diameters, and fission-gas release less than 1% of that generated. In addition, there was no evidence of structural change in the UO_2 when it was compared with unirradiated microstructures. The range of hydrogen concentration in the cladding of these fuel rods was 51 to 73 ppm; this represents only a very small increase in the hydrogen content when compared with a nominal content of about 40 ppm in the as-vacuum-annealed unirradiated cladding. All hydrides were in a random orientation. The range of oxide film thickness was 47 to 99 μin.

Results of irradiation tests of multicomponent tubular UO_2 fuel elements have been reported.[3] A tube-and-rod assembly was irradiated in a test loop in the Engineering Test Reactor (ETR) at a target maximum surface heat

*The LRD Program was discussed in Sec. V of *Power Reactor Technology*, 8(2).

flux of 320,000 Btu/(hr)(sq ft). During early stages of the irradiation, a burnout occurred which was the result of locally reduced coolant flow caused by a crossover of two thermocouples. A nested tubular element (tube-tube-rod) fabricated by vibratory compaction of UO_2 into 0.060-in.-thick Zircaloy-2 cladding, to densities in the range of 83 to 88% of the theoretical density, was irradiated at 350,000 Btu/(hr)(sq ft). After 10 reactor scrams and inadvertent severe thermal transients, fission-gas leakage was noted. Visual examination of the element failed to indicate defects. During disassembly of the components of the test elements, a fibrous material was found lodged between the rod and the inner tube and adjacent to a cladding failure. It was concluded that failure was induced by flow blockage caused by entrapped foreign matter. Extensive hydriding was noted at the cladding failure and further substantiated the postulated cause of failure. The appearance of the microstructure of both the fuel and the cladding in the region of the failure indicated that failure resulted from interference with surface heat transfer rather than from excessive local heat generation. A third element, containing the tube-tube-rod array similar to that described immediately above, was irradiated to its target burnup of 1360 Mwd per ton of UO_2 at a maximum surface heat flux of 400,000 Btu/(hr)(sq ft). Post-irradiation evaluations indicated that less than 10% of the fission gases and less than 50% of the sorbed gases were released.

Evaluation[4] of the influence of irradiation on the ductility of Zircaloy tubing by means of mechanical burst, weld-shear, and bend tests has indicated no effective loss in ductility after exposure to an integrated fast flux of 10^{20} neutrons/cm^2 at less than 100°C. Tubular fuel elements up to 2 ft long, with outside and inside diameters of about $2\frac{1}{4}$ and $1\frac{1}{2}$ in., were fabricated with Zircaloy-2 or low-nickel Zircaloy-2 cladding. The fuels used were vibratory-compacted and vibratory-compacted-and-swaged UO_2. The following conclusions are quoted from Ref. 4:

> The results of these tests indicate that large diameter tubular elements should not fail by either sheath rupture or weld separation due to irradiation embrittlement. In this event, calculations have shown that the limiting stress should be that stress required to cause sheath collapse. The tests also showed that the irradiation exposures, up to approximately 10^{20} nvt, had no noticeable effect on the sheath ductility, as measured by mechanical burst tests.
>
> These conclusions would be invalid, however, if severe hydriding, such as was previously observed in the . . . test series, were present.

Prototype fuel elements for the first Mobile Low Power Plant No. 1 (ML-1) core loading have been irradiation tested[5] in a gas-cooled General Electric Test Reactor (GETR) loop. The ML-1 core contains 61 fuel elements that are arranged in 61 pressure tubes located in the reactor calandria. Each fuel element contains 19 pins, with 1 unfueled pin in the center surrounded by two concentric rings containing 6 UO_2 and 12 BeO-UO_2 fuel pins. The objectives of these tests, in addition to providing irradiation performance data, included verification of design calculations concerning hot-spot limits and determination of in-pile corrosion resistance of Hastelloy X to the coolant gas. It was also noted[5] that the closed Brayton cycle used in the ML-1 plant was highly sensitive to pressure losses. For example, an increase of 1 psi in the system pressure drop resulted in a loss in net thermodynamic output of 6 kw. Hence another objective of the tests was to evaluate the influence of corrosion-product buildup or changes in fuel-element configuration on pressure drop.

The conditions in the gas loop are summarized below:[5]

Element power, kw	55
Inlet coolant temperatures, °F	800
Outlet coolant temperatures, °F	1200
Mass flow rate, lb/hr	1560
Loop operating pressure, psia	315

Two fuel elements, one of which was instrumented, were irradiated for 6415 hr in a coolant gas that was 99.5 wt.% N_2 and 0.5 wt.% O_2. The irradiation testing of the uninstrumented fuel element was continued in air for an additional 3736 hr.

Results[5] of cladding-temperature measurements indicated good agreement with previous calculations, and it was concluded that the hot-spot limit of 1750°F would not be exceeded at the full element power of 55 kw. Results of pressure-drop measurements during the test indicated no problems with respect to possible reductions in the net thermodynamic output of

the cycle. Postirradiation examination of the cladding microstructure indicated the formation of a massive second phase, which was due to an apparent reaction between nitrogen and Hastelloy X in all fuel pins that were instrumented. It was postulated that leaks were present at the brazed joints between the fuel and thermocouples and that the coolant gas permeated the inside of the fuel rods; nitrogen was measured in these rods. It was further postulated that the fuel gettered the O_2, leaving an oxygen-free N_2 atmosphere that reacted with the Hastelloy X to form a second phase which, in some cases, formed a continuous layer on the inside surface of the cladding and extended intergranularly through the thickness. All tubes that contained this second phase were severely embrittled. It was stated[5] that problems of this nature are not anticipated in the operating reactor.

The fuel pins in the 19-rod fuel assembly were spaced by means of spirally wrapped spacer wires on each pin. As a result of a 300°F difference in temperature between the fuel pin and the spacer wire, spiral bending of the fuel pins was observed, after irradiation, on a pitch that was almost the same as that of the wire wrap. It was concluded that the pin bending was a result of unequal expansion of the fuel pins and spacer wires.

An understanding of the performance of sodium-bonded hypostoichiometric UC fuels during transients has been obtained[6] through capsule testing in the Transient Reactor Test Facility (TREAT). Rods resembling the second Hallam fuel loading and containing 0.872-in.-diameter carbide fuel (4.58% carbon) clad with stainless steel of 0.952-in. outside diameter and 0.010-in. wall thickness were subjected to a total of five transients. A summary of results is given in Table III-1.

Evidence of uranium migration was not found even after bursts that provided fuel temperatures in excess of 2700°F. Bursts that increased the temperature to about 4200°F did not provide evidence of melting. However, a decrease in the amount of free uranium was noted, and it is postulated[6] that uranium became redissolved in the UC. Temporary boiling of the sodium, which probably occurred during the final transient, was rapidly quenched by cooler sodium located about the boiling region. The integrity of the fuel rod was such that it was concluded that "power levels of fuel rods of this type can reach values which are 100 times maximum steady-state levels for pulse duration of about 1 second without serious consequence."[6]

Incoloy 800 Cladding

Incoloy 800 is being evaluated[7] as a possible fuel-cladding material for use in nuclear superheat reactors. Procurement, quality control, fabrication, and metallographic evaluation of Incoloy 800 are described in detail in Ref. 7. Prior to 1962 there was little information on the fabrication of this material into thin-walled tubing.

Some of the first tubing received in the welded and drawn condition exhibited unhomogenized weld zones and disturbed surface layers. It was shown that the weld zone was a potentially weaker area than the base metal. It was concluded that the microstructure of all incoming Incoloy 800 tubing should show:[7]

1. No dendritic segregation in the weld zone.
2. Equal grain size in the weld zone and parent metal.
3. Grain size smaller than ASTM Number 5.

Complete recrystallization of the weld zone could be achieved by annealing in the tempera-

Table III-1 RESULTS OF TREAT TESTS* OF SODIUM-BONDED URANIUM CARBIDE FUEL RODS[6]

Transient number	TREAT energy, Mw/sec	Initial reactor period, sec	Peak central fuel temp. (measured), °F	Peak fuel temp.,† °F	Peak bond temp. (measured), °F	Peak pressure increase in fuel section, psi
1	30.7	0.259	1025	1060	845	3
2	63.3	0.157	1380	1520	980	8
3	180.0	0.158	2540	2760	1475	16
4	31.4	0.259	1030	1030	835	2
5	293.0	0.101	3970	4200	1840	20

*Initial temperature about 700°F; initial pressure about 32 psia (fuel section and inner capsule).
†Each value represents the maximum temperature at any position in the fuel since, as a result of flux depression, the peak transient temperature would not be expected to occur in the center of the fuel slug. Values are based on analog calculations and the measured central temperature.

ture range of 1900 to 2100°F, but the dendritic structure could only be eliminated after two cold reductions of approximately 20 to 30% followed by annealing at 2000 to 2100°F. The grain size could then be reduced by subsequent cold working and annealing.

The ductility of Incoloy 800 was reduced after 1000 hr at temperatures above 1050°F as a result of an aging phenomenon associated with the precipitation of titanium- and aluminum-containing intermetallics. As a result of this information, the titanium and aluminum content was specified as 0.1% maximum. Cold-worked Incoloy 800 was insensitive to annealing temperatures below 1000°F. Softening was initiated at 1400°F and was reasonably complete in 10 to 15 min at 1800°F. Rapid grain growth occurred at temperatures above 1850°F. Solution annealing occurred at 2050 to 2100°F after 1 to 2 hr. It was necessary to water quench through the 1100 to 1600°F temperature range in order to prevent carbide precipitation.

Typical chemical and physical properties for Incoloy 800 are indicated in Tables III-2 and III-3.

A monograph on the use of Incoloy 800 for fuel-element cladding has been prepared[8] which includes: mechanical properties, physical metallurgy, metallography and electron-microscopy techniques, radiation damage, strain-cycle fatigue, corrosion, and irradiation results of fuel elements (clad with Incoloy 800) exposed in the superheat environment. Performance in superheated-steam environments has been superior to that for the austenitic stainless steels, and Incoloy 800 has been selected as the reference cladding in some nuclear superheat applications.

Table III-2 CHEMICAL COMPOSITION[7] OF INCOLOY 800

Constituent	Weight percent
Nickel	30 to 35
Chromium	19 to 23
Iron	Balance
Carbon	0.10 maximum
Manganese	1.50 maximum
Sulfur	0.03 maximum
Silicon	1.00 maximum
Copper	0.75 maximum

Table III-3 MECHANICAL PROPERTIES OF EXTRUDED INCOLOY TUBES[7]

Condition	Tensile strength, 1000 psi	Yield strength (0.2% offset), 1000 psi	Elongation in 2 in., %
As extruded	75-105	25-50	50-30
Annealed	75-100	25-55	50-30

References

1. D. R. McClintock and C. J. Kubit, Fabrication and Irradiation of Stainless Steel Clad UO_2 Fuel Rods (The LRD In-Pile Chemical Shim Loop Experiment), USAEC Report WCAP-3734, Westinghouse Electric Corp., Atomic Power Division, April 1964.
2. L. R. Lynam, Metallurgical Examination of PWR Core 1 Blanket Fuel Rods at the End of the Third Seed Life, USAEC Report WAPD-TM-433, Bettis Atomic Power Laboratory, August 1964.
3. M. K. Millhollen, G. R. Horn, and W. J. Flaherty, Multicomponent Tubular UO_2 Fuel Element Irradiations, USAEC Report HW-80291, Hanford Atomic Products Operation, November 1963.
4. M. R. Louthan, Jr., Destructive Evaluation of Irradiated Zircaloy Sheathing, USAEC Report DP-888, Savannah River Laboratory, May 1964.
5. J. S. Brunhouse et al., Army Gas-Cooled Reactor Systems Program, USAEC Report IDO-28616, Aerojet-General Nucleonics, June 1964.
6. S. J. Stachura, M. Silberberg, and R. N. Cordy, Uranium Carbide Transient Heating Experiments — Phase 1, USAEC Report NAA-SR-9508, Atomics International, Aug. 1, 1964.
7. R. F. Kirby, D. F. Macmillan, and J. R. Punches, Fabrication of Fuel Cladding from Incoloy Alloy 800, An Evaluation of Methods, USAEC Report GEAP-4557, General Electric Company, Atomic Power Equipment Department, April 1964.
8. C. N. Spalaris (Comp.), Incoloy-800 for Nuclear Fuel Sheaths (A Monograph), USAEC Report GEAP-4633, General Electric Company, Atomic Power Equipment Department, July 1964.

Section

IV

Power Reactor Technology

Components

Liquid-Metal-Level Probes

Some significant improvements have been made in resistance type probes for determining the level of high-temperature liquid metals in a vessel. Reference 1 reports on an investigation of the various types of probes that can be used for determining the level of liquid metals and concludes that the resistance type is promising. The J probe that was developed utilized a tube with alumina-insulated stainless-steel-clad nickel wires. A straight tube probe, similar in operation and construction to the J probe, but which indicates one discrete level only and is called an I probe, also was studied.

The J probe indicates the level of the liquid metal over the range from the top of the unsupported leg of the J to the bottom of the J. This is accomplished by passing a direct current through one of the insulated internal wires in the tube to the tip of the J as shown in Fig. IV-1. The negative wire from the power supply is connected to the metal vessel. A potential is then impressed between the tip of the J and the vessel and the resistance between these two points is changed as the liquid-metal level around the unsupported leg is changed. The maximum resistance exists when the level is lowest, and the current must pass through the sheath of the J tube. The potential between the tip of the J and the tank is measured by a second insulated internal wire to the tip of the J and a wire to the tank. Unfortunately the resistances of the stainless-steel sheath and the probe wires vary with temperature. In the design shown in Fig. IV-1, compensation is accomplished by maintaining a constant voltage across the entire probe and internal current lead. Figure IV-2 is a refinement of this design wherein the temperature-compensation circuit is connected inside the J tube and the resistance of the current lead is increased. The increased length of the lead is in the same temperature gradient as the probe, and compensation is obtained by maintaining a constant voltage between the tip of the probe and the internal splice.

The I probe, which indicates whether the liquid-metal level is above or below a certain point, is shown in Fig. IV-3. A potential is impressed between the end of the probe and the vessel, and an amplifier connected in parallel to this circuit actuates a relay to signify that the level of the liquid metal is below the probe end. When the liquid metal comes in contact with the end of the probe, a new circuit with less resistance is established and the decrease in voltage causes the amplifier to drop the relay.

In addition to the problem of attaining correct temperature compensation, there is a problem of obtaining thermoelectric voltage if

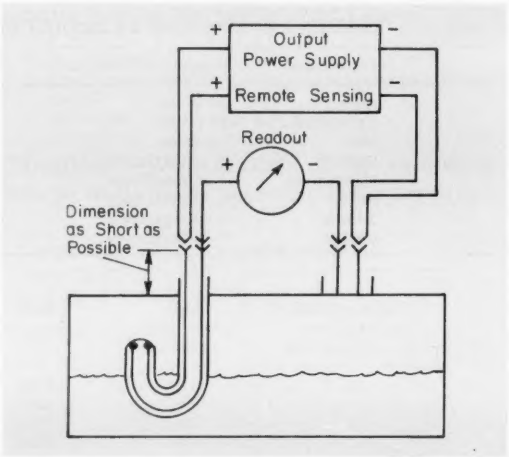

Fig. IV-1 Two-wire J probe with externally connected temperature-compensation circuit.[1]

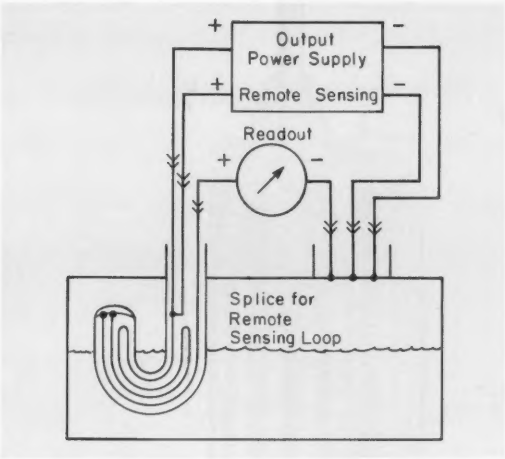

Fig. IV-2 J-probe design with internally connected temperature-compensation circuit and increased-resistance remote sensing loop.[1]

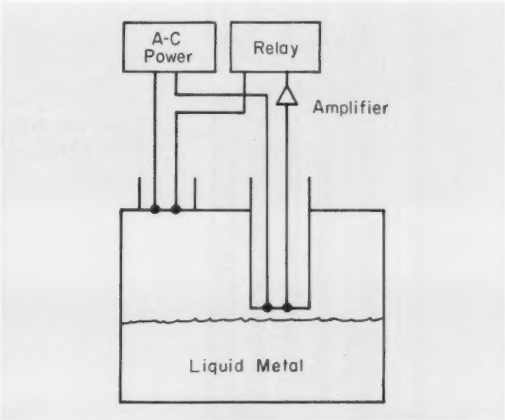

Fig. IV-3 I probe for one-point-level determination.[1]

materials are not carefully selected. Further, complete wetting of the surface of the probe requires careful attention to the preparation of the surface before immersion. Reference 1 indicates that if the probe can be completely wetted, an accuracy within 1% can be achieved.

Pressure-Tube Fretting Corrosion

A continuing surveillance program is being conducted on the Plutonium Recycle Test Reactor (PRTR) to monitor fretting corrosion of the pressure tubes. A summary of results of (1) programs designed to detect and determine the extent of in-reactor fretting attack and (2) associated tests outside the reactor is presented in Ref. 2. The PRTR[3] is a heavy-water-moderated pressurized-heavy-water-cooled reactor that operates at 70 Mw(t). The moderator is contained at low pressure and temperature in an aluminum calandria tank, with 85 calandria tubes arranged vertically. Zircaloy-2 pressure tubes, containing fuel assemblies, are installed in the calandria tubes. The coolant enters the bottom of the pressure tubes at a temperature of 248°C and a pressure of 1090 psig and discharges at the top at 277°C and 1080 psig. The maximum flow rate per pressure tube is 123 gal/min. The Zircaloy-2 pressure tubes are 3.250 in. in inside diameter, with a minimum wall thickness of 0.146 in. The tubes are flanged at the upper end to permit attachment of outlet-nozzle jumper assemblies and are tapered at the bottom for attachment of inlet jumpers. Before installation the pressure tubes were autoclaved to provide a zirconium dioxide surface film.

The fuel assemblies are 19-rod clusters, as shown in Fig. IV-4, and both metallic (aluminum-plutonium) and ceramic (UO_2 and PuO_2-UO_2) Zircaloy-2-clad rods are used. Spacing between rods is maintained with top and bottom brackets and spirally wound spacer wires around the outside of selected fuel rods. The aluminum-plutonium and the PuO_2-UO_2 fuel assemblies are bound with circumferential bands, whereas a wire wrap is used on the UO_2 fuel assembly. A pressure tube containing a fuel assembly is shown in Fig. IV-5. The fuel assembly is attached to an upper hanger that is supported near the outlet nozzle and is free to expand downward. Clearance between the fuel assembly and the pressure tube is a nominal 0.015 in., but it can be as much as 0.050 in. Portions of the fuel assembly that could come in contact with the pressure tube include the following: the three equidistant centering feet on both the top and bottom end brackets; the wire wrap (bundle or individual rods); circumferential bundle bands if the centering feet are sufficiently worn; and the individual fuel rods if the wire wraps and centering feet are sufficiently worn.

A rather comprehensive program[4–6] has been conducted, on a continuing basis, to determine

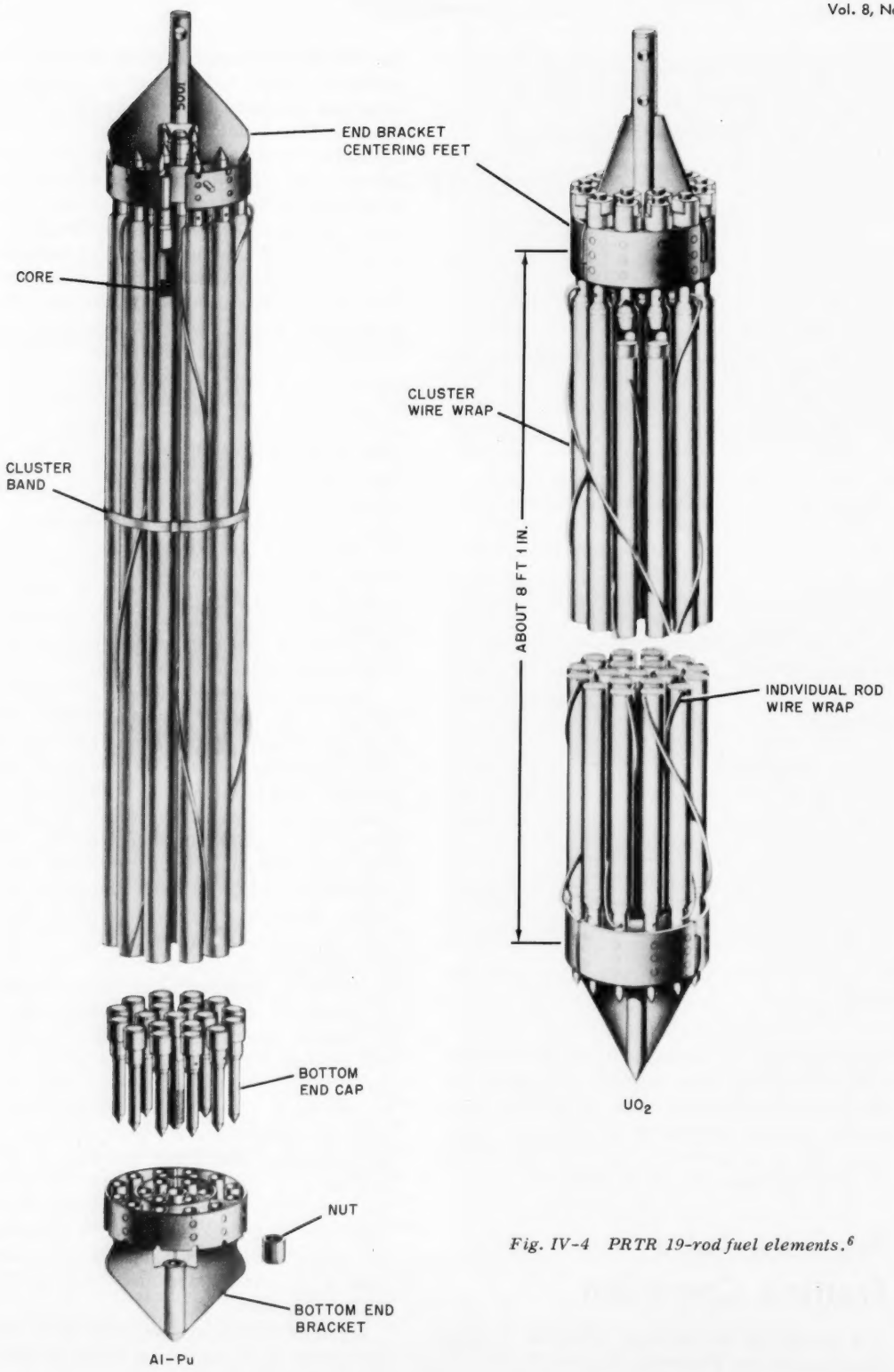

Fig. IV-4 PRTR 19-rod fuel elements.[6]

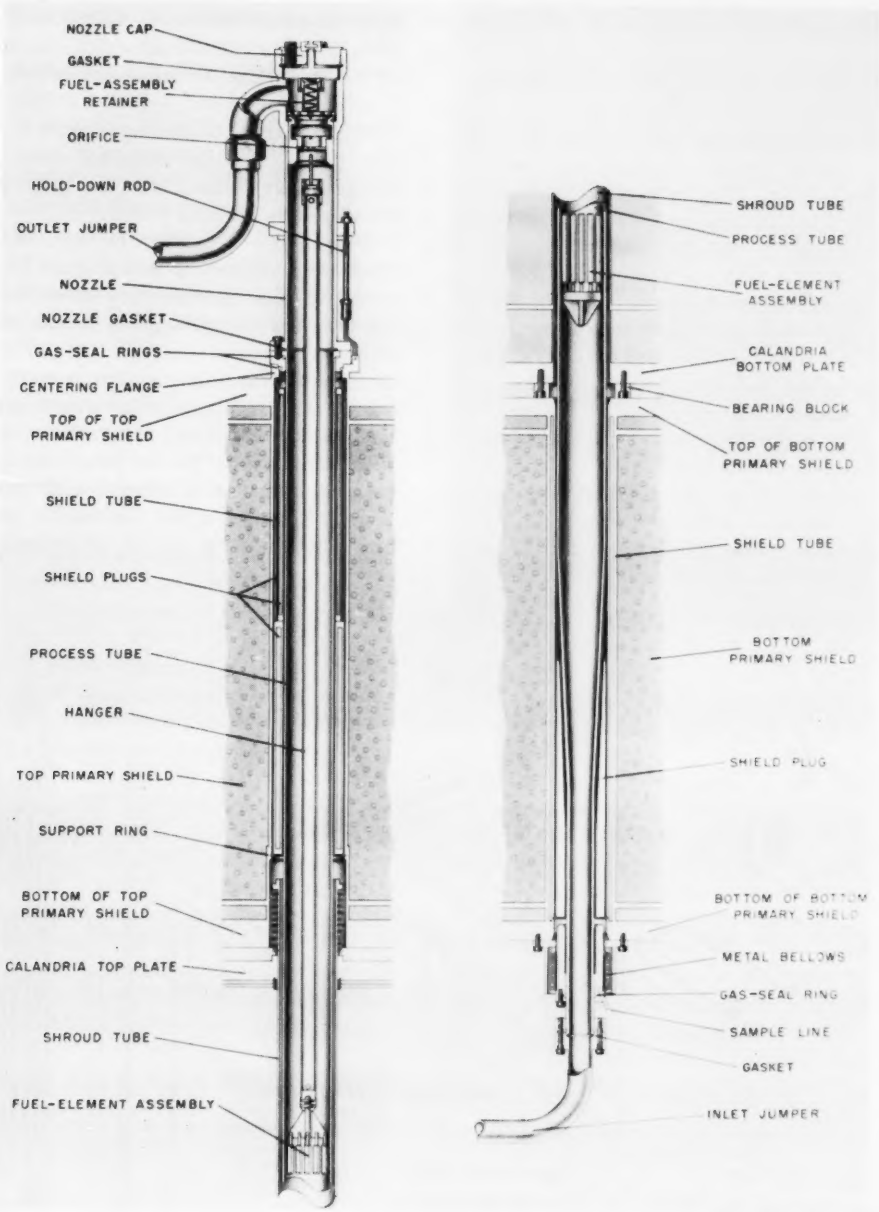

Fig. IV-5 Pressure-tube assembly.[2]

the magnitude of fretting corrosion and to establish methods of minimizing pressure-tube wear. The program consisted of out-of-reactor tests and in-reactor examination. The initial phase of the out-of-reactor program consisted of flow tests in a high-temperature high-pressure facility and autoclave tests. The initial test specimen was a Zircaloy-2 tube with a spirally wound Zircaloy-2 wire. The wire was fastened at one end and was free at the other end. After two weeks of exposure in recirculating water at 300°C and 25 ft/sec, grooves approximately 0.001 to 0.005 in. deep were noted on the tube, and the wire was worn approximately 0.020 in. where the moving wire could contact the stainless-steel housing. This and other similar tests showed that the relative movement induced by flow could result in localized corrosion areas at the point of contact between two surfaces. Sliding- and impact-wear tests were conducted in autoclaves in deionized water at 1500 psi. The sliding-wear test, consisting of a rotating disk in contact with a stationary rod, showed that disk penetration and rod wear increased with increasing temperature in the range from 100 to 400°C. The test also showed that the wear increased with contact pressure from 5 to 15 psi and also with rotational speed of the disk. The impact-wear test consisted of a solenoid-activated cylindrical plunger tipped with Zircaloy-2 impacting against a Zircaloy-2 flat plate. Results indicated over twice the plunger wear with an increase in the water temperature from 200 to 400°C.

An out-of-reactor test facility, shown in Fig. IV-6, was utilized to test an individual reactor pressure-tube fuel-element assembly at operating flow and temperature. Fretting marks found after facility operation prompted additional tests in vertical test sections. Initial tests were conducted with a Zircaloy-2 collar mounted at the bottom of a steel rod suspended in a tube lined with Zircaloy-2. The fretting attack was found to be independent of water velocity in the range from 15 to 30 ft/sec but quite sensitive to clearance between the three centering feet on

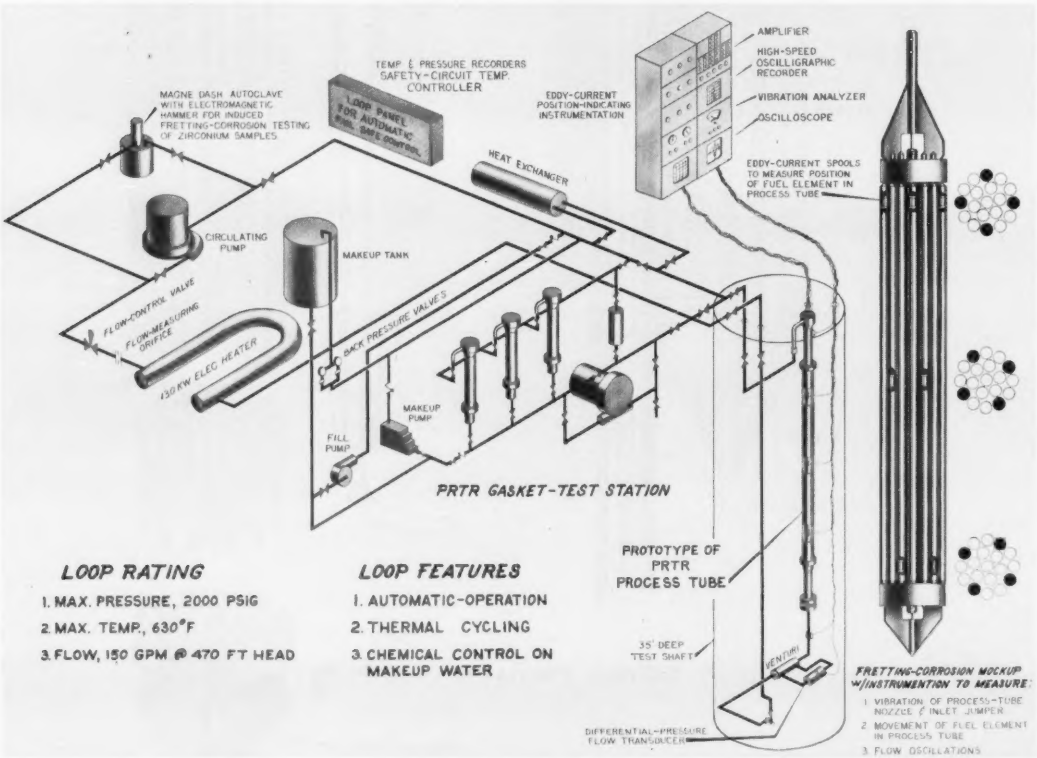

Fig. IV-6 Out-of-reactor test facility.[2]

the collar and the tube. The attack also increased with temperature and with a superimposed external vibrating force. Later tests were conducted in a vertical test assembly consisting of the upper 10 ft of a PRTR pressure tube containing a fuel assembly. Water at 300°C was circulated upward through the fuel assembly at at a flow rate of 123 gal/min. After two weeks fretting marks, approximately 0.005 in. deep, were noted at the contact points between the pressure tube and the centering feet of the fuel-assembly end brackets. Continued testing did not always increase the depth of penetration, indicating that the process may be intermittent. Increasing the contact surface tended to decrease the penetration.

The out-of-reactor tests generally have shown that fretting attack is increased with increased temperature, vibration, and clearance. The process seems to be one of removing the protective oxide film mechanically and thus permitting progressive oxidation of the Zircaloy.

The in-reactor examination of the condition of the pressure tubes consisted of visual inspection and measurement of the depth of observed marks.[4–6] A television-camera–borescope arrangement was used to examine the inner surface of the pressure tube and to read a dial indicator used to measure the depth of marks. The number and location of fretting marks are given in Table IV-1, and an example of one of the more severe fretting marks is shown in Fig. IV-7. This mark was detected during an examination of all the pressure tubes in May and June of 1962. The diagonal fretting mark is the result of contact with a wire wrap around a fuel assembly and is approximately 0.025 in. deep. The wire wrap was worn sufficiently to allow two of the fuel rods to contact the tube wall, and the vertical fretting mark resulted.[5]

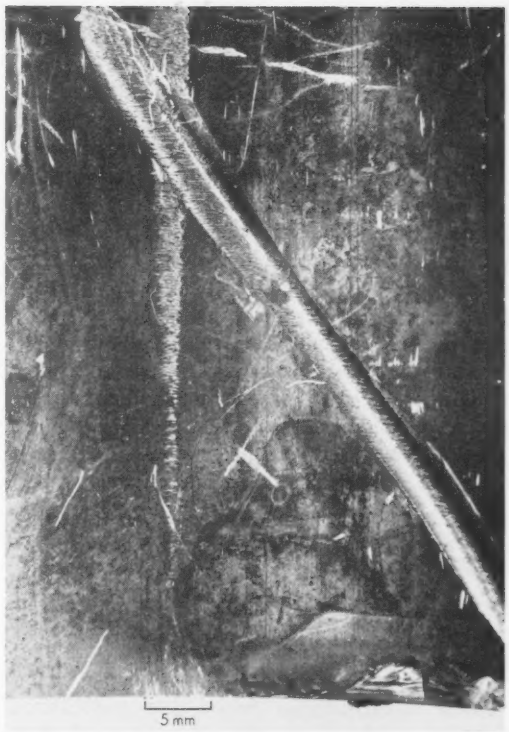

Fig. IV-7 Pressure-tube fretting mark.[2]

The severity of fretting corrosion has decreased as some of the causes have been discovered and corrected. For example, the width of the centering feet on the fuel assemblies has been increased on new fuel, and this has decreased the severity of the fretting.[6] Some of the fretting was attributed to a failed flow-straightening baffle, which has been replaced. Tests are continuing to define more precisely the reasons for fretting attack and to find methods for minimizing or eliminating this

Table IV-1 NUMBER AND LOCATION OF PRESSURE-TUBE FRETTING MARKS[2]

Fuel-element component making mark	9/60 to 6/62*		7/62 to 11/63*		Total*	
	No.	%	No.	%	No.	%
Centering feet, upper end bracket	327	20.0	418	24.2	745	22.1
Centering feet, lower end bracket	484	29.6	524	30.3	1008	30.0
Wire wraps	674	41.2	788	45.5	1462	43.5
Unclassified	150	9.2	1		151	4.4
	1635	100.0	1731	100.0	3366	100.0

*Includes marks found on tubes that have been removed from the reactor.

problem. Techniques are under development for continuous monitoring of PRTR pressure tubes to detect excessive fretting attack — for example, monitoring of the zirconium content of the water shows some promise.[7] Of the analytical methods available (emission spectrographic, radiochemical, and spectrophotometric), emission spectrography is considered most reliable for measuring zirconium contents as low as 0.10 ppb. Work is continuing on the correlation of the results of this technique with fretting attack. Recently a vibration-monitoring program has also been started. Velocity type transducers have been installed on the inlet jumpers of selected pressure tubes; sufficient data have not been obtained as yet to enable a correlation between vibration measurements and zirconium concentration in the coolant water.

References

1. S. J. Fanciullo, Development of Liquid Metal Level Probes, USAEC Report PWAC-423, Connecticut Aircraft Nuclear Engineering Laboratory, April 1964
2. W. K. Winegardner, Fretting Corrosion in the Plutonium Recycle Test Reactor, USAEC Report HW-80021, Hanford Atomic Products Operation, March 1964.
3. N. G. Wittenbrock, P. C. Walkup, and J. K. Anderson, Plutonium Recycle Test Reactor Final Safeguards Analysis, USAEC Report HW-61236, Hanford Atomic Products Operation, Oct. 1, 1959.
4. D. R. Doman and P. J. Pankaskie, In-Reactor Monitoring of Zircaloy-2 PRTR Pressure Tubes, Part I, September 1960–May 1962, USAEC Report HW-73701(Rev.), Hanford Atomic Products Operation, May 1962.
5. D. R. Doman and P. J. Pankaskie, In-Reactor Monitoring of Zircaloy-2 PRTR Pressure Tubes, Part II, May and June 1962, USAEC Report HW-74731, Hanford Atomic Products Operation, August 1962.
6. P. J. Pankaskie, In-Reactor Monitoring of Zircaloy-2 PRTR Pressure Tubes, Part III, July 1963–November 1963, USAEC Report HW-80158, Hanford Atomic Products Operation, December 1963.
7. T. F. Demmitt, Zirconium Concentration Measurements in the PRTR Primary Coolant: Interim Report, December 8, 1962 to June 30, 1963, USAEC Report HW-78080, Hanford Atomic Products Operation, July 1963.

Section

V

Power Reactor Technology

Specific Reactor Types

Sodium-Graphite Reactors: Steam Cycles

A recent steam-cycle optimization study[1] has been made for sodium-graphite nuclear power plants to determine optimum steam conditions and sodium-system parameters for plants in the 350- to 400-Mw(e) size range. The general results are summarized as follows:

1. For plant ratings up to approximately 350 Mw(e), a 2400-psig steam pressure results in the most economical operating condition.
2. For plant ratings above 350 Mw(e), a 3500-psig steam pressure results in the most economical operating condition.
3. The highest justifiable initial and reheat steam temperatures are 1000°F each for reheat cycles at a reactor outlet temperature of 1150°F.
4. For most economical operation the sodium temperature rise across the reactor should be in the range of 350 to 375°F.
5. For the 2400-psig steam cycle, the most economical log mean temperature differential of the intermediate heat exchanger is 65 to 80°F. For the 3500-psig steam cycle, this range is 85 to 95°F.

The optimum (most economical) cycles for a fuel-cycle cost of $0.20 per 10^6 Btu and a reactor sodium outlet temperature of 1150°F, in the 400-Mw(e) size, are summarized in Table V-1.

In this study heavy emphasis was given the steam portion of the plant, inasmuch as the costs of the reactor and related sodium systems are relatively insensitive to the steam pressure used, once the outlet sodium temperature for the reactor has been fixed. The major components of the power-generating system considered are shown schematically in Fig. V-1, along with typical sodium and steam temperatures and pressures.

The steam-cycle study was divided into three phases. During phase I studies were made for steam pressures of 1450, 1800, 2400, and 3500 psig for a 350-Mw(e) plant. The basis of comparison was the total evaluated cost, made up of major-equipment costs and capitalized energy costs.

Bases are given in Ref. 1 for costs of such items as heat-exchanger surfaces, feedwater

Table V-1 CHARACTERISTICS OF OPTIMUM STEAM CYCLES FOR 400-Mw(e) PLANTS[1]

	7% capital-charge rate	14% capital-charge rate
Steam throttle pressure, psig	3500	3500
Initial and reheat steam temperatures, °F	1000 each	950 each
Type of steam cycle	Double reheat	Double reheat
Type of steam turbine (last-stage blading size)	Cross compound double flow (30 in.)	Tandem compound four flow (30 in.)
Net station heat rate, Btu/net kw-hr	7665	7870
Fuel-cycle cost at $0.20 per 10^6 Btu, mills/net kw-hr	1.53	1.57
Reactor sodium ΔT, °F	350	350
Intermediate heat exchanger log mean temperature difference, °F	95	95

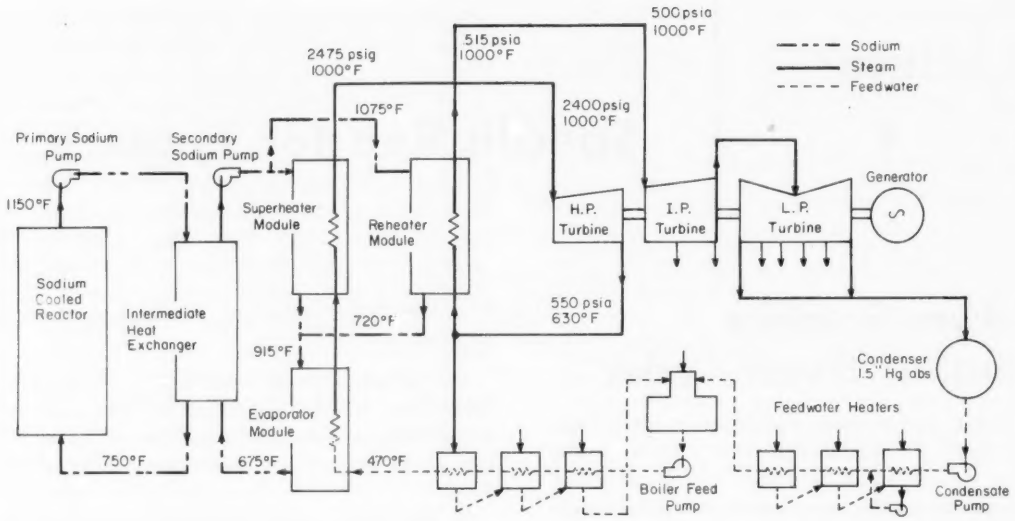

Fig. V-1 Typical schematic of sodium-graphite nuclear power-generating system.

heater-supply and treatment systems, and the steam-condensate systems. Variations in reactor thermal rating due to changes in cycle efficiency were accounted for by use of a reactor cost differential of $50,000 per 1% change in reactor rating. For the phase I study, all fuel-cycle costs were based on $0.20 per 10^6 Btu. Other assumptions used for evaluating fuel-cycle costs are also presented.[1]

Phase I results are summarized as follows:

1. The steam-pressure condition with the lowest cost at a 14% capital-charge rate is 2400 psig; the next best pressure is 3500 psig.

2. At a 7% capital-charge rate, the steam-pressure condition with the lowest cost is 3500 psig, followed by the 2400-psig pressure condition.

3. At a 14% capital-charge rate, the best steam-temperature condition is 950°F; at a 7% capital-charge rate, either 950 or 1000°F is recommended.

During phase II a system pressure of 2400 psig was used for a more detailed study of various parameters of a 350-Mw(e) plant.

The following summarizes phase II results:

1. A 350°F sodium-temperature differential across the reactor is optimum.

2. A 65 to 80°F log mean temperature difference for the intermediate heat exchanger is optimum.

3. Although the cross-compound turbine generators with 1800-rpm low-pressure sections are more efficient and provide improved turbine-cycle heat rates over the tandem-compound machines at 3600 rpm, the significantly higher cost of the cross-compound unit more than offsets the savings in operating costs for $0.20 per 10^6 Btu fuel costs.

4. The optimum feedwater temperature is 475°F.

5. As fuel costs increase from $0.20 to $0.25 per 10^6 Btu, the trend is toward the more efficient cycle (steam pressure of 2400 psig and initial and reheat steam temperatures of 1000°F).

6. As the plant-capacity factor decreases from 80 to 60%, the trend is to the less efficient cycle (steam pressure of 2400 psig and initial and reheat steam temperatures of 950°F.

7. It is difficult to justify the added capital cost of high-pressure feedwater heaters for feedwater temperatures above 475°F with $0.20 per 10^6 Btu fuel costs.

In phase III the basic effort was to study in detail the merits of 2400- vs. 3500-psig steam for a 400-Mw(e) plant with 14 and 7% capital-charge rates. For these studies the reactor-sodium outlet temperature was held at 1150°F. Areas investigated were generally similar to those in phase II.

Results for the phase III study are summarized as follows:

1. The 3500-psig double-reheat plant with 1000°F steam temperatures and a 7% capital-charge rate provides savings of $1,485,000 over the 2400-psig case.

2. The 3500-psig plant with 950°F steam temperatures and a 14% capital-charge rate appears to provide savings of $292,000 and $444,000 for single and double reheat, respectively, over the single-reheat case with 2400-psig steam. However, additional analyses would be required to verify this trend.

3. A 1050°F steam temperature is not justified for any steam-pressure condition studied.

4. The tandem-compound four-flow turbine with a 30-in. last-stage blade is the best selection at 14% capital-charge rates: the cross-compound double-flow unit with a 43-in. last-stage blade is the best with the 7% capital-charge rate.

Naturally any generalized study of this kind can be only as valid as the assumptions on which it is based, and the author of Ref. 1 has pointed out the need for basing the steam conditions in an actual plant design upon the specific site and ground rules as related to a specific utility company. It is also well to recognize that optimum conditions are strongly affected by the particular designs of some of the components in the sodium system.

The economic results of the study would not apply to other sodium-cooled reactors because the effects of changes in reactor capital costs and fuel costs were not investigated over a wide range. For example, the much lower fuel cost of a sodium-cooled fast reactor plant would tend to justify lower steam-cycle temperature conditions and therefore lower optimum cycle efficiencies than those found for the sodium-graphite case.

Reference

1. G. A. Schneider, Steam Cycle Optimization Study for Large Sodium Graphite Nuclear Power Generating Stations, USAEC Report NAA-SR-9488, Atomics International, Aug. 31, 1964.

Section

VI

Power Reactor Technology

Unconventional Approaches

Fast Supercritical Water Reactor

As a part of the continuing study effort for the U. S. Atomic Energy Commission's Division of Reactor Development, Hanford Atomic Products Operation issued a report by Aase et al.[1] describing the design and economic evaluation of a 300-Mw(e) fast supercritical-pressure water reactor. The fast supercritical-pressure power-reactor (FSPPR) design employed a fast breeder-reactor concept, a plutonium-uranium fuel cycle, and supercritical water as the coolant. Hanford has been involved in the design of supercritical-pressure power reactors for some time, and an earlier design,[2] the supercritical-pressure power reactor (SPPR), was reviewed in *Power Reactor Technology*, 6(3): 73-78 June (1963). The SPPR is quite different in design than the FSPPR in that it is a thermal reactor employing UO_2 as the fuel material. The earlier work was utilized in the preparation of Ref. 1, however, to establish the design of the auxiliary systems for the FSPPR.

The FSPPR was designed for a power of 677 Mw(t) with a net efficiency of 44.3%. The reactor core is fueled with plutonium and uranium oxides with a moderator-segmented-core design and axial and radial blankets. The moderator-segmented-core design was expected to overcome some of the safety considerations that must be dealt with in a fast reactor design and will be discussed shortly. A direct-cycle system provides supercritical-pressure water coolant with turbine-inlet conditions of 3500 psig and 1050°F. Figure VI-1 shows a simplified feedwater-and-steam-system schematic for the FSPPR. It can be seen that two stages of reheat are employed using regenerative heat exchangers and a cross-compound turbine. The reactor incorporates three coolant passes with temperature control at the inlet to the second and third passes. This coolant-temperature-control system was intended primarily to compensate for the changes in power distribution expected during the life of the core. Shown in Fig. VI-2 are one reactor core, a portion of the piping, and the containment vault. The containment vault is designed to contain two reactors in a tandem arrangement. This tandem arrangement allows refueling of one core while the other core is in operation, although simultaneous operation of the two cores was not intended. It was felt that this type of design should reduce reactor downtime quite significantly and thereby increase the productive period of the plant. A single FSPPR core was designed for approximately 4.9 full-power years, equivalent to approximately 6.1 calendar years. The volume between the two main reactor vaults in Fig. VI-2 is a basin to be used in fueling operations. One of the FSPPR cores can be seen in the upper portion of the figure; below the reactor core is the fuel-transfer pot to be used in refueling. A series of headers is placed at the top of the reactor-core assembly to deliver and remove the supercritical coolant from the various passes of the reactor core. Numerous jumper assemblies are utilized, a few of which are shown in Fig. VI-2, to connect the toroidal headers to the core fuel assemblies.

The internal composition of the core can be seen in Figs. VI-3 and VI-4. The cross section of the core in Fig. VI-3 shows the two core regions that are refueled with uranium oxide and plutonium oxide and separated by an absorber region that contains moderator tanks. The control rods for the core are located in the moderator tanks, and a radial blanket is

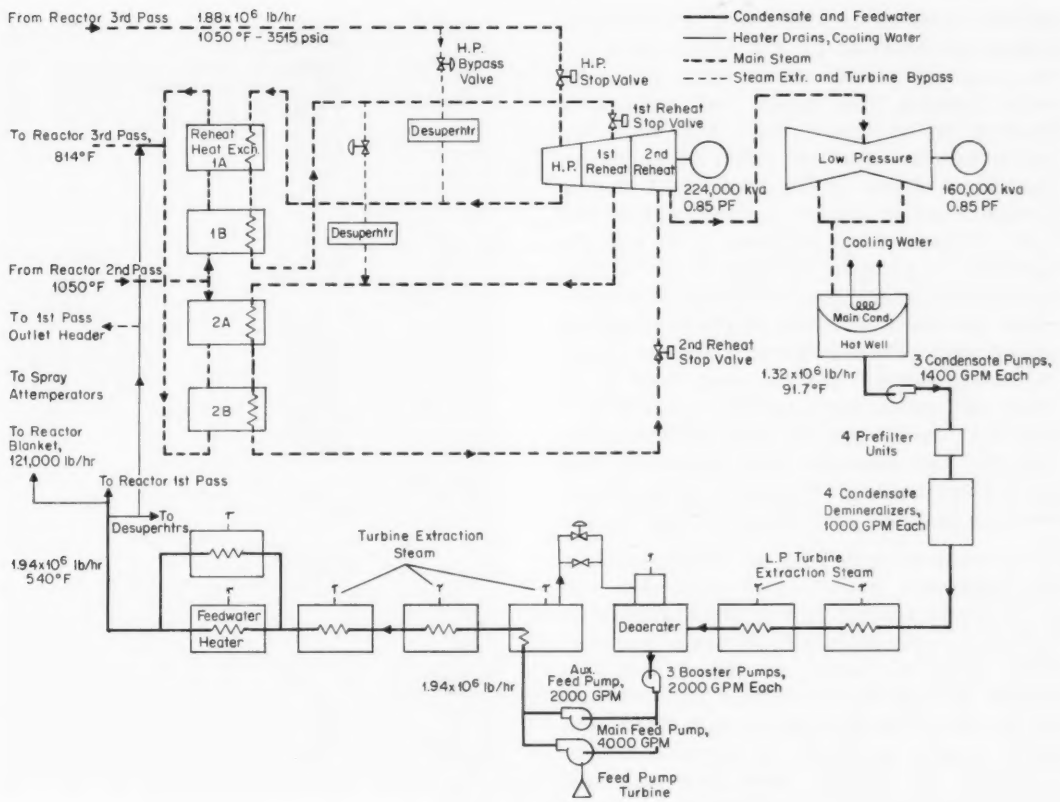

Fig. VI-1 Simplified feedwater and steam system of the FSPPR.

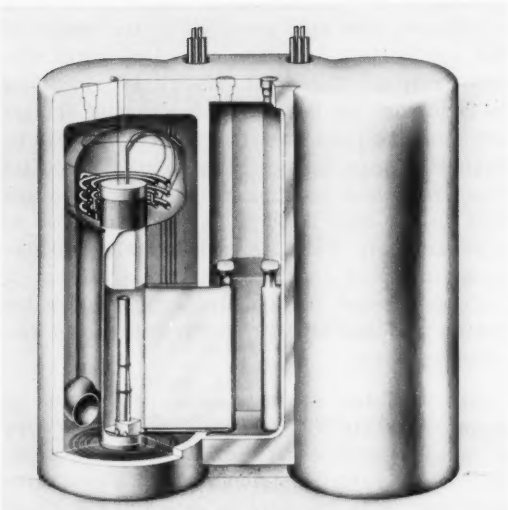

Fig. VI-2 The FSPPR.[1]

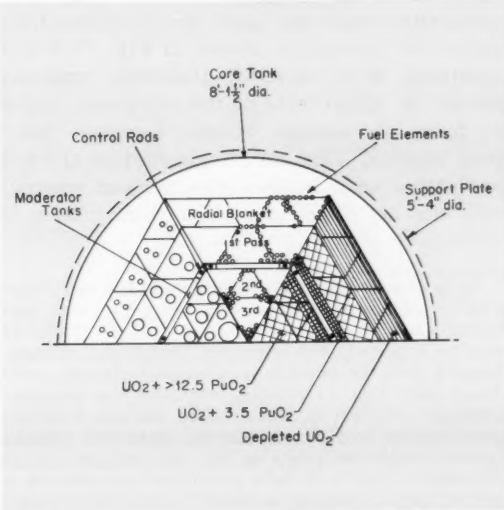

Fig. VI-3 Core layout of the FSPPR.[1]

placed around the core assembly. Three coolant passes are provided for the central section of the core, and coolant also is delivered to the radial blanket. The upper and lower axial blankets can be seen in Fig. VI-4. These fuel assemblies are provided either in equilateral triangular shapes or in trapezoidal shapes. Coolant flows to the fuel elements at the outer rows of tubes of the elements, flows down the elements to a mixing chamber at the bottom, and returns up the central portion of the element. The top and bottom of the elements are closed with porous plugs to allow the escape of fission gases.* The fastening plate on the inlet and outlet fuel-element pipes is connected to the top support plate of the reactor, with the fuel elements being suspended from the reactor top support plate. The characteristics of the FSPPR are given in Table VI-1.

The nuclear design of the FSPPR utilized the previously mentioned moderator-segmented-core concept to overcome some of the difficulties associated with the use of a moderating material, water, as the coolant. The amount of water in the reactor core was kept as low as possible to maintain a sufficiently hard neutron spectrum to permit economic operation. The use of a moderator-segmented core reduced the interaction between the coolant and the neutrons by enhancing the internal leakage effect of the core. The coolant flow was arranged such that the lower density flow occurred at the center of the core. The core composition that was used for the moderator-segmented design is shown in Fig. VI-3 and consisted of a layer of absorbing material placed on either side of the moderator tanks to form an annular volume between "fast" core regions. This core segmentation allowed productive core leakage upon coolant voiding, with the net effect of coolant voiding being a reduction of reactivity. A negative flooding coefficient was also provided in the design by the appropriate selection of fuel-to-water volume ratios. The total calculated reactivity behavior of the core as a function of coolant inventory is presented in Fig. VI-5. It can be seen that near the operating point the coolant reactivity void coefficient is nearly zero and that in the fully flooded condition the core is approximately 9% $\Delta k/k$ subcritical. Calculations indicated that a considerable amount of hydrogen could be lost from the moderator region and the coolant coefficients would remain negative.

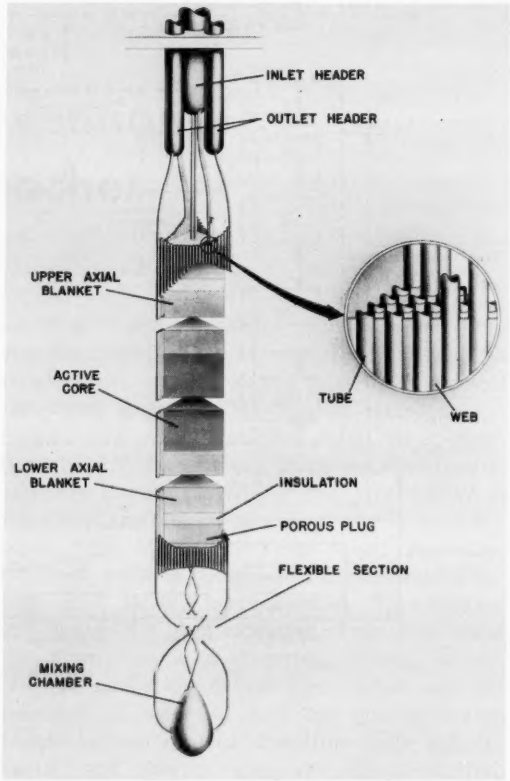

Fig. VI-4 Fuel-element assembly of the FSPPR.[1]

The detailed nuclear core description is shown in Table VI-2. At the center of the core a mean fission energy of 82 kev was calculated. The radial distribution of the mean fission energy in the core is shown in Fig. VI-6, and the calculated initial and end-of-life radial power distributions are shown in Fig. VI-7.

*It is expected that, in order for fast breeder reactors to compete with existing reactors, high fuel burnups of the order of 80,000 to 100,000 Mwd/ton may be required. The resulting fission-gas release, coupled with the potentially weakened cladding condition after long irradiation, magnifies the internal-pressure problem in fuel-element design. Fission-gas volumes provided to accommodate this release become large and unwieldy for the compact cores envisaged. Faced with these problems some designers are talking of concepts in which "controlled venting" of fuel-element fission gases would be employed. Gases would be collected and separated from the cover gas and processed.

Table VI-1 CHARACTERISTICS OF THE CONCEPTUAL FAST SUPERCRITICAL-PRESSURE POWER-REACTOR (FSPPR) PLANT

General characteristics

Thermal power, Mw	677
Net electric power, Mw	300
Net efficiency, %	44.3
Gross efficiency, %	47.1
Auxiliary power, Mw	2.83
Equivalent main feed-pump power, Mw	9.93

	General	First pass	Second pass	Third pass	Radial blanket
Reactor dimensions					
Outside dimension of each region, in.		34.8	22.8	13.3	43.5
Core height, in.	60				
Core + axial-blanket height, in.	75¾				
Core volume, liters	3095				
Flux-trap thickness, in.	~8.75				
Reactor fuel inventory					
Depleted uranium, kg	30,895				15,407
Total plutonium, kg	1559				
Fissile plutonium, kg	1059				
Reactor power density, kw/liter of core + blanket	218.7				
Reactor specific power, kw/kg of uranium + plutonium	50				
Fuel-element assembly					
Fuel material	PuO_2 + depleted UO_2				
Initial enrichment, % plutonium		14.5	12.5	12.5	
Fuel density, g/cm³	9.3				
Flux-trap material	PuO_2 + depleted UO_2				
Enrichment, % plutonium	3.8				
Fuel-element type	Equilateral triangle or trapezoid				
No. of fuel elements	72	18	18	6	30
No. of cooling tubes per fuel element		1216	686	730	43
Fuel-element active length, ft	5				
Fuel-element overall length, ft	15.25				
Cooling-tube material	René 41				
Cooling-tube inside diameter, in.		0.146	0.160	0.204	0.286
Cooling-tube wall thickness, in.		0.013	0.022	0.027	0.030
Cooling-tube spacing, in. (on triangular pitch)		0.291	0.269	0.358	1.20
Weight of fuel per fuel element, lb of oxide		1544	523	906	1132
Fuel-cladding material	René 41				
Cladding thickness, in.		0.090	0.083	0.080	0.090
Heat removal					
Maximum heat flux, Btu/(hr)(sq ft) ($\times 10^{-5}$)	8.93	8.73	7.00	6.43	
Average heat flux, Btu/(hr)(sq ft) ($\times 10^{-5}$)	2.91	2.98	2.27	4.14	
Average core power density, kw/liter	230				
Maximum fuel temperature, °F	2260	2260	1740	1930	
Maximum pressure-tube temperature, °F	1385	1300	1385	1320	

Table VI-1 (Continued)

	General	First pass	Second pass	Third pass	Radial blanket
Coolant conditions					
Pass inlet temperature, °F		514	804	820	
Pass outlet temperature, °F		804	1050	1050	
Pass inlet pressure, psig		4360	4330	4100	
Turbine throttle pressure, psig	3515				
Coolant flow rate, lb/hr × 10^{-6}	1.88				
Coolant pH	8.7 to 9.0				
Nuclear characteristics					
Core life					
Full-power years	4.85				
Calendar years	6.06				
Average fuel irradiation level at discharge, Mwd/metric ton	83,700	69,160	96,840	122,500	
Initial fuel isotopic composition					
^{239}Pu, % of total plutonium	55				
^{240}Pu, % of total plutonium	32				
^{241}Pu, % of total plutonium	13				
Neutron lifetime, sec	8.7×10^{-7}				
Effective neutron fraction	0.0041				
Final fuel isotopic composition					
^{239}Pu, % of total plutonium		63.0	64.0	54.6	
^{240}Pu, % of total plutonium		28.0	25.0	32.1	
^{241}Pu, % of total plutonium		9.0	11.0	13.3	
Initial flux-trap enrichment, % plutonium	3.8				
Final flux-trap enrichment, % plutonium	5.2				
Fuel-temperature effect, mk	−20				
Other temperature effects, mk	2				
Total safety-rod strength, mk	50				
Total control-rod strength, mk	25				
Breeding ratio, core + blankets	1.14				
Moderator characteristics					
Moderator material	YH_x or $ZrH_x + H_2O$				
YH_x or ZrH_x, vol.%	70				
Reactor heat in moderator, Mw	1.3				
Control					
No. of control rods	6				
Control-rod material	Stainless steel−1.25% natural boron				
Control-rod diameter, in.	3/4				
No. of safety rods	6				
Safety-rod material	Stainless steel−1.10% B^{10}				
Safety-rod diameter, in.	3/4				
Coolant	H_2O (same as used for moderator)				
Power-cycle components					
Turbine type	Cross compound				
No. of reheats	2				
High-pressure-stage conditions, °F/psi	1050/3515				
First-reheat conditions, °F/psi	1000/912				
Second-reheat conditions, °F/psi	1000/299				
Exhaust pressure, in. Hg	3.5				
Condenser size, sq ft	110,000				
No. of feedwater stages, including deaerator	7				
No. of feedwater pumps	2				

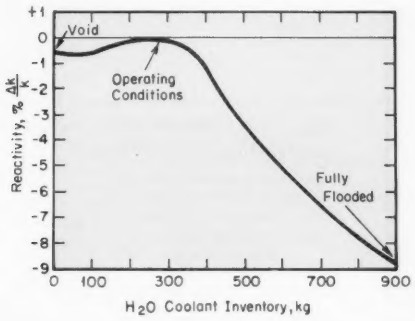

Fig. VI-5 Reactivity change vs. coolant inventory for the FSPPR.[1]

although differences in reactivity values indicate that perhaps diffusion theory gave more conservative results."

In calculating the pressure drops of the fuel-element cooling channels, it was determined that a large variation between the minimum and maximum pressure drops within an element existed; however, when the maximum pressure drop was used, the calculated core total pressure drop was 658 psi, and the total pressure drop across the reactor, including turbine reheat exchanges and associated piping, was about 800 psi. The heat-transfer correlations of Chalfant* were used at pressures above

Table VI-2 NUCLEAR CORE-DESIGN DATA[1]

Region	Radius, cm	Description	Enrichment, % plutonium	Coolant pass	Coolant density, g/cm³	Composition, vol.%				
						Fuel	Coolant	Tube	Wall	Void
1	30.8	Third reactor core	12.5	3	0.108	46.4	30.9	18.4	1.7	2.6
2	44.2	Second reactor core	12.5	2	0.121	46.0	30.7	18.4	1.9	3.0
3	51.2	Absorber region, low plutonium enrichment	3.8	2	0.121	46.0	30.7	18.4	1.9	3.0
4	54.2	Zirconium hydride moderator, water cooled		Low-pressure water		70, ZrH_x	30			
5	61.2	Absorber region, low plutonium enrichment	3.8	1	0.445	63.9	21.3	12.8	0.9	1.1
6	80.4	First reactor core	14.5	1	0.445	63.9	21.3	12.8	0.9	1.1
7	100.4	Depleted uranium	0.0	1	0.445	85.9	5.7	2.2	2.9	3.3

The dimensions and worths of the control and safety rods are presented in Table VI-1. Some radial enrichment zoning was done in the absorber region to reduce power peaking in this region over core lifetime. A fuel-temperature coefficient of reactivity was computed for the Doppler broadening of the ^{238}U resonances only as $-2 \times 10^{-5}\,\Delta k/(k)(°C)$. It was recognized that a further positive contribution to the fuel-temperature coefficient would be available from ^{239}Pu and that a negative contribution would be available from ^{240}Pu; however, these were not calculated. Fuel- and cladding-expansion effects were estimated to be approximately $10^{-6}\,\Delta k/(k)(°C)$. The majority of the static reactor-physics calculations were done utilizing diffusion-theory codes, and some checking of the validity of diffusion theory for a core of this type with a moderator region located internally was done using a multigroup transport code. The results[1] obtained from the two methods of calculations "... generally confirmed the data yielded by diffusion theory, 4000 psia. Similarly the correlation of McAdams* was used at pressures from 3500 to 4000 psia. The maximum heat flux in all cases was limited by the pressure-tube wall temperature.

The proposed refueling scheme involves fueling one of the tandem reactors before the other reactor is shut down. The newly loaded reactor then begins operation while the exposed fuel is allowed to decay for a period of two to three months in the reactor core. The fluid jumpers for the individual fuel elements are remotely cut, and the fuel elements are transferred to the fuel storage basin. Plugs are then placed in severed coolant jumpers until the time of refueling, at which time the jumpers are temporarily frozen with liquid nitrogen and the coolant jumpers of the new fuel elements are welded in place. Removal of the frozen coolant

*The reader may wish to refer to Refs. 7 and 8 of Ref. 1 for these correlations.

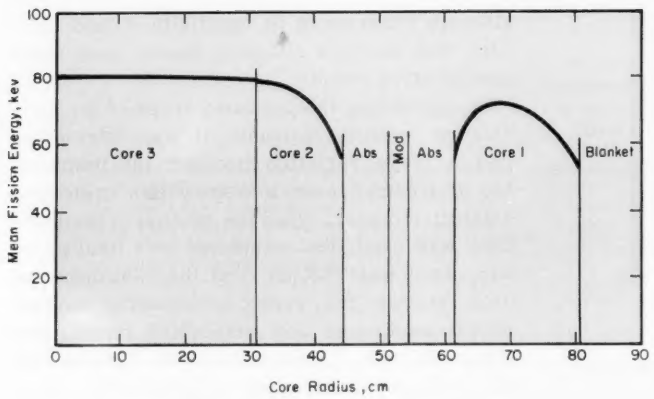

Fig. VI-6 Mean-fission-energy distribution in the FSPPR.[1]

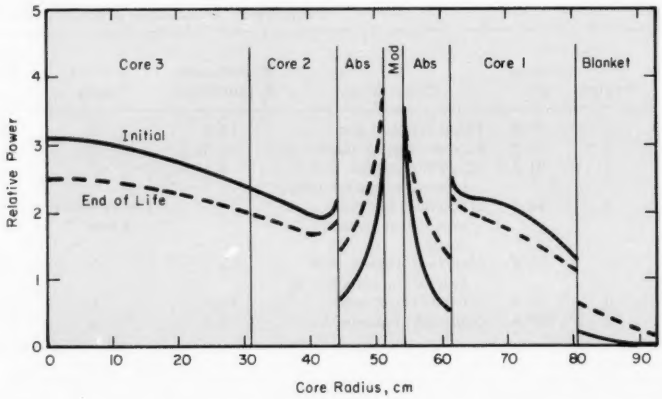

Fig. VI-7 Power distribution in the FSPPR.[1]

then restores the function of the coolant passages.

Startup of the reactor involves first purging the water in the coolant channels with low-density steam to reduce the large shutdown margin. The approach to criticality is made by control-rod withdrawal, and on reaching criticality the design power is approached by simultaneously programmed manipulations of rod position, pressurization, and flow. During normal operation the load changes are accomplished by positioning of the turbine admission valve, and the reactor power level is automatically adjusted, using a banked-control-rod configuration, to hold the coolant outlet temperature constant. Additional control and safety systems are provided to ensure safe operation at power.

The power-generation costs that were computed for the FSPPR are shown in Table VI-3. The cost data given in the "Guide to Nuclear Power Cost Evaluation" handbook were used to arrive at the computed unit cost of power generation of approximately 5.12 mills/kw-hr.

The following required technological developments are enumerated:[1]

(1) Analytical and experimental verification of a practical and economical moderator segmented core design.

(2) Demonstration of the Doppler effect as a reliable prompt negative coefficient in fast ceramic-fueled reactors.

(3) Demonstration of a high endurance (greater than 80,000 Mwt days per tonne) internally cooled ceramic-fueled element.

(4) Development of high strength alloys and fabrication techniques for complex pressure tube assemblies that are reliable under high exposures and fast neutron irradiation.

(5) Development of water treatment cleaning and decontamination techniques that avoid fouling and carry-over problems in a once through cooling system.

(6) Demonstration of reliable and economical remote fuel and pressure piping replacement methods.

Table VI-3 POWER-GENERATION COSTS FOR FSPPR[1]

	Capital cost, $	Rate, %	Annual cost, $	Unit cost,* mills/kw-hr
Fixed charges				
Depreciating capital				
Total capital cost (less land)	51,373,000	14.46	7,429,000	3.534
Nondepreciating capital				
Land and land rights	360,000	13.0	47,000	0.022
Working capital				
Plant operation and maintenance	130,000	13.0	17,000	0.009
Fuel-cycle operations	4,015,000	13.0	522,000	0.248
Nuclear liability insurance			280,000	0.133
Subtotal: fixed charges			8,295,000	3.946
Operating costs				
Operating and maintenance cost			889,000	0.423
Fuel cost			1,572,000	0.748
Subtotal: operating costs			2,461,000	1.171
Total power-generation costs			10,756,000	5.117

*Plant factor is 80%.

Hanford Graphite Superheat Reactor

The N-Reactor Project Section of the Hanford Atomic Products Operation[3] has recently reported results of a design and evaluation study for a Hanford graphite superheat reactor (HGSR). These studies involved consideration of two basic reactor sizes, a 300-Mw(e) plant and a 1000-Mw(e) plant, both utilizing pressurized process tubes, vibratory-compacted uranium dioxide fuel, graphite-moderator blocks, and a once-through boiling-superheating coolant passage.* Since the 1000-Mw(e) plant design is quite similar to the smaller plant design, a detailed description of the smaller plant will be presented first, followed by some indications of the differences that were encountered in the design of the larger plant.

The process tubes, fuel elements, and coolant routing are shown in Fig. VI-8, and further descriptive material is presented in Table VI-4. As shown in Fig. VI-8, the process tube would be supported by the top primary shield, and the seal assembly on the fuel element would transmit the load of the fuel to the nozzle. This seal assembly would separate the 400°F water that enters the fuel element and flows down its outer peripheral flow channel from the steam that passes up the central flow channel of the element and exhausts from the nozzle assembly. The tube that separates the water and steam is formed in a 360° helix around the fuel-element supporting rod, thereby eliminating the need to penetrate the steam-tube wall. Subcooled water passes down the outer flow channel, and then the boiling water returns up the two inner annuli where it is further vaporized and superheated. A 10-mil Incoloy cladding is proposed for the fuel that would be uranium dioxide vibratorily compacted to approximately 92% of the theoretical density. The process tubes would be manufactured from Zircaloy (in the active core region) and stainless steel (above the core).

The general arrangement of process tubes, control rods, graphite stack, and coolant-flow zones is shown in Fig. VI-9. Further information is contained in Table VI-4. As shown in Fig. VI-9, the graphite stack is composed of horizontal layers of blocks of graphite with successive layers oriented at right angles to each other. The process tubes and the continuous-chain control rods then pass through the openings provided for them in the graphite stack. The dimensions of the graphite blocks are such that ventilating voids are provided

*These designs bear some similarities to the graphite-moderated superheating reactor located at the USSR Beloyarsk Power Station. This reactor was described in *Power Reactor Technology*, 8(1): 28-34 (Winter 1964–1965), and the reader may wish to refer to that review for a comparison. Some of the major differences in the two designs involve the general mechanical arrangement of the fuel, the fuel enrichment, and the coolant-flow-passage arrangement.

throughout the graphite stack, which would serve as steam vent volumes in the event of a process-tube rupture. Steam would escape through the core by the lifting of the layer of the stack in which the rupture occurred. Steam would then travel to a plenum located in the reflector which could carry the steam outside the reactor block. The top, bottom, and side reflectors are also composed of graphite, and they maintain the same basic layer formation with the exception that the steam-vent spaces are filled with graphite to increase the reflecting ability. Thermal and biological shields are arranged around the graphite stack. Flow to the process tubes would be controlled in 5 flow-control zones (shown in Fig. VI-9). Each of the 5 zones is divided into two halves that are supplied by headers located on opposite sides of the reactor. Each flow-control zone would theoretically contain tubes of equal power; thus by supplying a control valve on each of 10 supply headers, flow control could be maintained to one-half of a zone. Fuel charging and discharging would be managed along the same zone plan.

The locations of the control-rod blocks are also shown in Fig. VI-9. The control-rod design incorporates a flexible endless chain, with poison sections attached to it, and a bottom drive that would be supplied power by a hydraulic motor. This particular flexible rod design provides for a minimum of storage height when the poison is out of the reactor and also allows assistance from gravity in holding the control material in the reactor. Dimensional details and other information on the control rods are in Table VI-4. Cooling water would be supplied to the tubes containing the control rods, and poison could be injected into the rod coolant passages for backup reactivity control; a flow diagram of the poison system is shown in Fig. VI-10.

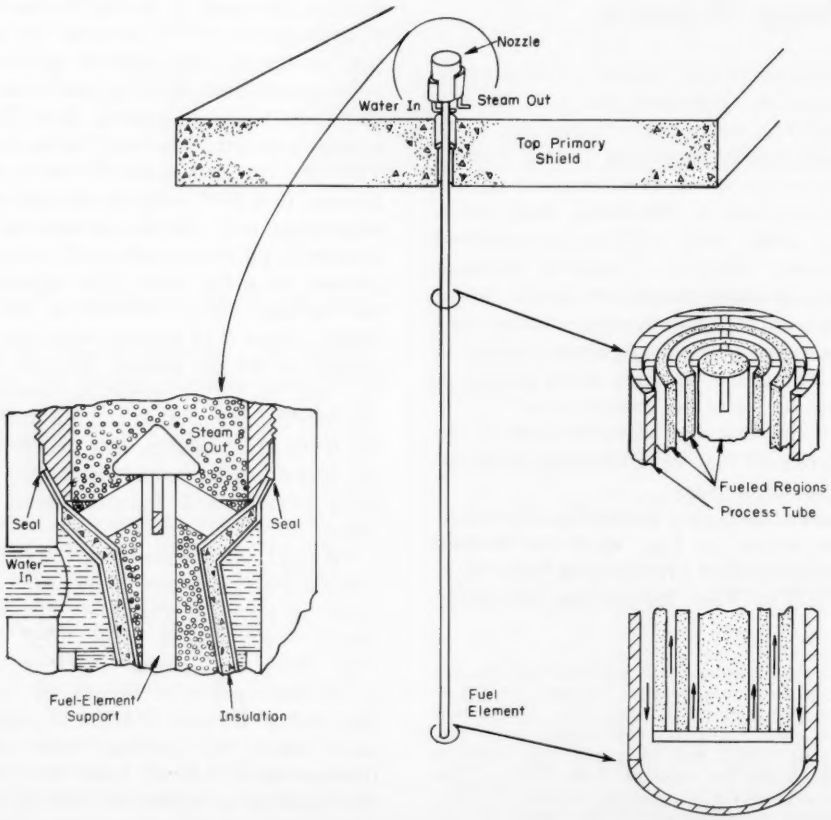

Fig. VI-8 Reentrant type process-tube coolant connections in the HGSR.[3]

Table IV-4 DATA SUMMARY FOR 300- AND 1000-Mw(e) HGSR PLANTS[3]

	300-Mw(e) plant	1000-Mw(e) plant
Gross thermal, Mw(t)	840	2700
Gross electrical, Mw(e)	321	1030
Net electrical, Mw(e)	311	1000
Exit steam condition	1100 psig, 1000°F	Same
Inlet steam condition	1525 psig, 400°F	Same
Steam flow, lb/hr	2.48×10^6	8.10×10^6
Reactor Description		
Reactor core		
Active width, ft	~18	~28
Active length, ft	~18	~26
Lattice spacing, in.	9.25	10.5
Total UO_2 loading, kg	50,600	156,000
Fuel initial enrichment	2.391 wt.%	2.37 wt.%
Reflector material	Graphite	Same
Reflector thickness	2 ft 11½ in.	2 ft 10½ in.
Fuel element		
Fuel material (~92% of theoretical density)	UO_2	Same
Fuel-element dimensions (UO_2), in.		
Outer cylinder	OD, 2.279 ID, 1.690	OD, 2.644 ID, 2.055
Inner cylinder	OD, 1.457 ID, 0.80	OD, 1.603 ID, 0.950
Rod diameter	0.50	0.490
Cladding material (base case)	Incoloy	Incoloy
Cladding thickness, in.	0.010	Same
Process-tube material	Zircaloy-2	Same
Process-tube dimensions, in.	ID, 2.475 Wall, 0.234	ID, 2.907 Wall, 0.275
Reactor-control material	Boron steel	Same
No. of control elements	64	140
Control-rod OD, in.	1.5	Same
Control-rod effective length, ft	18.2	26
Reactor mass velocities (average), lb/(hr)(sq ft)		
Boiler pass	1.22×10^6	1.38×10^6
Superheat pass	1.06×10^6	9.46×10^5
Reactor bulk-coolant inlet temperature, °F	400	Same
Reactor maximum coolant outlet temperature, °F	1115	Same
Steam coolant flow, lb/hr	2.48×10^6	8.10×10^6
Maximum fuel temperature, °F	4100	4700
Maximum cladding temperature, °F	1200	1260
Maximum heat flux, Btu/(hr)(sq ft)(°F)		
Boiler pass	4.70×10^5	4.88×10^5
Transition pass	4.84×10^5	5.21×10^5
Average heat flux, Btu/(hr)(sq ft)(°F)		
Boiler pass	2.09×10^5	2.17×10^5
Transition pass	2.15×10^5	2.32×10^5
Peak-to-average power ratio		
Axial	1.5	Same
Radial	1.5	Same
Relative radial flux distribution in fuel element		
Outer cylinder	1.29	Same
Inner cylinder	1.08	Same
Rod	1.00	Same
Average core velocity, ft/sec		
Inlet	6.5	7.2
Outlet	200	195

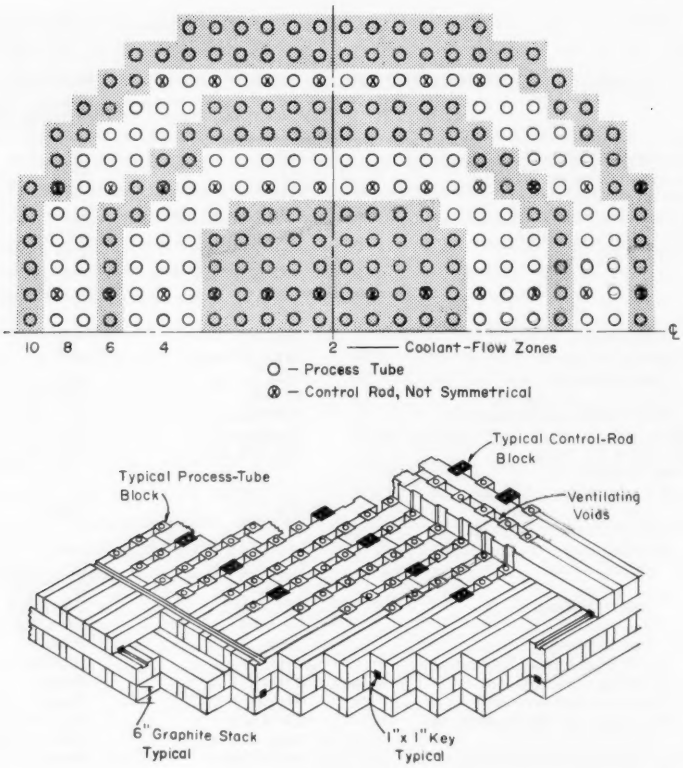

Fig. VI-9 General arrangement of fuel, control rods, graphite stack, and coolant-flow zones in the HGSR.[3]

The IBM-7090 program FLEX-II was used to obtain most of the physics analysis. The computed operational reactivity variations and reactivity coefficients are shown in Table VI-5. Control requirements are minimized because of an assumed staggered discharge scheme wherein about 10% of the fuel would be discharged at a time; a fuel exposure of 22,000 Mwd/ton would be obtained. As reported in Ref. 3: "... If the reactor is loaded with 2.39% enriched material, its reactivity will exceed the capacity of the control system. Therefore, some poison must be charged in the new reactor ..." It is proposed[3] that natural uranium dioxide elements be used as control material to be periodically replaced with the reference enrichment until the equilibrium fuel-management phase is achieved. Computed peak-to-average power ratios are included in Table VI-4.

The flow diagram for the steam- and feedwater-supply system, as well as for some of the auxiliary systems, is shown in Fig. VI-10. A helium-gas system is supplied for the HGSR to provide a chemically stable environment for the process tubes and the graphite moderator and to provide a means of detecting small steam or water leaks within the pile. The helium would also serve as a carrier of corrosion inhibitors to protect the process tubes from gas hydriding. Analytical instruments are provided in the gas loop to control the carbon monoxide and the water-vapor level. During the initial 20 sec following scram or shutdown, cooling would be provided by the coastdown of the feedwater pump; thereafter a shutdown-cooling system takes over. The fuel-element-rupture monitoring system consists of a gamma spectrometer, which analyzes gas from the primary coolant, and a delayed-neutron detector. Location of the particular process tubes containing ruptured fuel would be by means of traps located in each outlet nozzle. Superheated steam flows to the 1800-rpm tandem

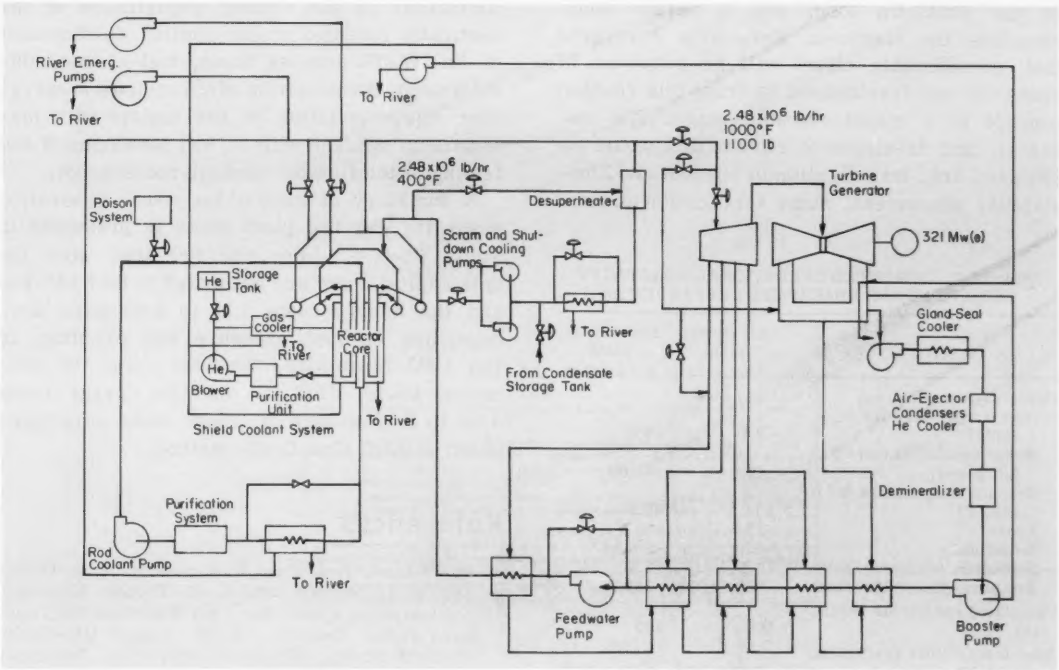

Fig. VI-10 Flow diagram of the 300-Mw(e) HGSR.[3]

compound turbine with inlet conditions of 1000°F and 1100 psig.

As previously mentioned, the 1000-Mw(e) design is quite similar to, and in many instances identical to, the smaller design. Only those differences which are considered significant will be mentioned here. The flow diagram shown in Fig. VI-10 is the same as the schematic for the 1000-Mw(e) plant with appropriate changes made in the various ratings. Table VI-4 describes some of the parameters that were changed in the 1000-Mw(e) plant. The length of the uranium-bearing section of the fuel elements was increased to slightly over 26 ft, the active width of the core was increased to approximately 28 ft, additional control rods were added, and the coolant flow was divided into three flow-control zones. Computed operational reactivity variations and reactivity coefficients for the 1000-Mw(e) HGSR are shown in Table VI-5. The larger design required doubling the capacity of the liquid-poison system, and this was accomplished by installing two systems identical to the ones used in the smaller plant. The circulation rate of the helium-gas system was doubled for the larger design; this maintained the same gas velocity through the reactor and the same frequency of gas exchange within the reactor. Steam for the larger unit would be supplied to two turbine-generators at the same inlet-throttle conditions. Nuclear control instrumentation would utilize the same low-level and intermediate-level systems; however, eight power-level channels would be utilized.

The HGSR was designed to operate at approximately a constant load; therefore the reactor operation would be at an approximately constant pressure and temperature. Manual control-rod movement would be used for level-load operations. The procedure that was envisioned for the cold startup involved maintaining the reactor flow rate at its normal operating value during the startup. The startup was estimated to require approximately 4 hr; the hot startup was estimated to require approximately 1 hr. Normal shutdown would be accomplished by gradual power reduction and corresponding flow reduction with steam going through the bypass to the turbine condenser. When the power level was approximately 10% of full power, the cooldown would be transferred

to the shutdown loop, and a scram would complete the shutdown. Reference 3 reports that considerable effort will be required in research and development to bring this reactor concept to a manufacturable stage. The research and development efforts that would be required are: investigation of burnout and flow-stability phenomena, some verification and optimization of the venting capabilities of the vertically oriented stack, limited development of the HGSR process tubes, fuel-element development, investigation of corrosion and carryover characteristics of the coolant with materials in contact with it, and development and testing of the flexible-control-rod concept.

A summary of some of the power-generation costs for the two plant sizes is presented in Table VI-6. "... For the 300 Mwe size, the unit capital costs are estimated to be $147/kw, and the energy costs 5.13 to 5.60 mills/kwh, depending on fuel exposure and cladding. In the 1000 Mwe size, the unit costs are estimated to be $112/kw and the energy costs 4.04 to 4.43 mills/kwh. These costs were computed by AEC Cost Guide method."

Table VI-5 COMPUTED OPERATIONAL REACTIVITY VARIATIONS AND REACTIVITY COEFFICIENTS*

	300-Mw(e) plant	1000-Mw(e) plant
Reactivity transient, mk		
Inlet temperature (68 to 400°F)	−9.5	−9.4
Power escalation (zero to full power)	−22.5	−39.6
Graphite temperature (68 to 1085°F)	29.5	32.5
Xenon	−26.9	−30.4
Samarium	−6.3	−6.3
Neptunium (plutonium holdup)	−3.4	−3.4
Exposure (22,000 Mwd/ton)	−320.0	−280.0
Calculated rod worths (total), mk	109	120
Inlet-temperature coefficient,* $\Delta k/(k)(°F)$	-2.85×10^{-5}	-2.82×10^{-5}
Power coefficient,*† $\Delta k/(k)$(Mw)	-2.74×10^{-5}	-1.43×10^{-5}
Graphite coefficient,* $\Delta k/(k)(°F)$	2.90×10^{-5}	3.20×10^{-5}

*These values are at "average" conditions, i.e., in a reactor containing fuel of all exposures from 0 to 22,000 Mwd/ton.

†This includes effects of water density and fuel temperature.

References

1. D. T. Aase, J. C. Fox, R. J. Hennig, R. E. Peterson, S. L. Stewart, and K. G. Toyoda, Economic Evaluation of a 300-Mwe Fast Supercritical Pressure Power Reactor, USAEC Report HW-78953, Hanford Atomic Products Operation, December 1963 (first unrestricted distribution, April 1964).
2. H. Harty, J. J. Regimbal, K. G. Toyoda, and R. D. Widrig, Economic Evaluation of 300-Mw(e) Supercritical Pressure Power Reactor, USAEC Report HW-68420(Rev.), Hanford Atomic Products Operation, June 1961.
3. Hanford Atomic Products Operation, Hanford Graphite Superheat Reactor (HGSR), Design Study and Evaluation, USAEC Report HW-73130, January 1960.

Table VI-6 POWER-GENERATION COSTS FOR 311-Mw(e)* AND 1000-Mw(e) HGSR PLANTS

		311-Mw(e)* plant			1000-Mw(e) plant		
	Rate, %	Capital cost, $1,000	Annual cost, $1,000	Unit cost, mills/kw-hr	Capital cost, $1,000	Annual cost, $1,000	Unit cost, mills/kw-hr
Fixed charges							
Depreciating capital							
Total capital cost (less land and land rights)	14.5	45,810	6,640	3.04	112,100	16,260	2.32
Nondepreciating capital							
Land and land-rights working capital	13.0	360	47	0.02	360	47	0.01
Plant operating and maintenance	13.0	159	21	0.01	540	70	0.01
Fuel-cycle operation	13.0	2,100	273	0.13	4,490	584	0.08
Nuclear liability insurance			289	0.13		340	0.05
Annual fixed charges, subtotal			7,270	3.33		17,301	2.47
Operating costs							
Operating and maintenance			890	0.41		2,280	0.32
Fuel cost			3,020	1.39		8,760	1.25
Operating costs, subtotal			3,910	1.80		11,040	1.57
Total power-generation costs			11,180	5.13		28,341	4.04

*The exact value of 311 Mw(e) was used in computing these costs instead of the rounded-off "300 Mw(e)" that appears throughout this article.

NUCLEAR SCIENCE ABSTRACTS

The U. S. Atomic Energy Commission, Division of Technical Information, publishes *Nuclear Science Abstracts (NSA)*, a semimonthly journal containing abstracts of the literature of nuclear science and engineering.

NSA covers (1) research reports of the U. S. Atomic Energy Commission and its contractors; (2) research reports of government agencies, universities, and industrial research organizations on a world-wide basis; and (3) translations, patents, books, and articles appearing in technical and scientific journals.

Complete indexes covering subject, author, source, and report number are included in each issue. These are cumulated quarterly, semiannually, and annually providing a detailed and convenient key to the literature.

Availability of *NSA*

SALE *NSA* is available on subscription from the Superintendent of Documents, U. S. Government Printing Office, Washington, D. C., 20402, at $30.00 per year for the semimonthly abstract issues and $22.00 per year for the four cumulated-index issues. Subscriptions are postpaid within the United States, Canada, Mexico, and all Central and South American countries, except Argentina, Brazil, British and French Guiana, Surinam, and British Honduras. Subscribers in these Central and South American countries, and in all other countries throughout the world, should remit $37.00 per year for subscriptions to semimonthly abstract issues and $25.00 per year for the four cumulated-index issues.

EXCHANGE *NSA* is also available on an exchange basis to universities, research institutions, industrial firms, and publishers of scientific information. Inquiries should be directed to the Division of Technical Information Extension, U. S. Atomic Energy Commission, P. O. Box 62, Oak Ridge, Tennessee, 37831.

TECHNICAL PROGRESS REVIEWS may be purchased from Superintendent of Documents, U. S. Government Printing Office, Washington, D. C., 20402. *Isotopes and Radiation Technology* at $2.00 per year for each subscription or $0.55 per issue; the other four journals at $2.50 per year and $0.70 per issue. The use of the coupon below will facilitate the handling of your order.

POSTAGE AND REMITTANCE: Postpaid within the United States, Canada, Mexico, and all Central and South American countries except as hereinafter noted. Add $0.50 per year, or $0.15 per single issue for the *Isotopes and Radiation Technology* journal and $0.75 per year or $0.20 per single issue for the other four journals for postage to all other countries, including Argentina, Brazil, British and French Guiana, Surinam, and British Honduras. Payment should be by check, money order, or document coupons, and MUST accompany order. Remittances from foreign countries should be made by international money order, or draft on an American bank, payable to the Superintendent of Documents, or by UNESCO book coupons.

order form

SUPERINTENDENT OF DOCUMENTS
U. S. GOVERNMENT PRINTING OFFICE
WASHINGTON , D. C., 20402

Enclosed:
document coupons ☐ check ☐ money order ☐

Charge to Superintendent of Documents No. _____

Please send a one-year subscription to

☐ NUCLEAR SAFETY
☐ POWER REACTOR TECHNOLOGY
☐ REACTOR FUEL PROCESSING
☐ REACTOR MATERIALS
(Each subscription $2.50 per year; $0.70 per issue.)
☐ ISOTOPES AND RADIATION TECHNOLOGY
(Each subscription $2.00 a year; $0.55 per issue.)

SUPERINTENDENT OF DOCUMENTS
U. S. GOVERNMENT PRINTING OFFICE
WASHINGTON, D. C., 20402

(Print clearly)

Name _____

Street _____

City _____ Zone ____ State _____